Spring 5-9-2020

Synthesis and Characterization of PAMAM-Fatty Acid “Janus-type” Dendritic Hybrids for Biomedical Applications

Abigail Grace Barker

Synthesis and Characterization of PAMAM-Fatty Acid "Janus-type" Dendritic Hybrids for Biomedical Applications

By
Abigail Grace Barker

A thesis submitted to the faculty of The University of Mississippi in partial fulfilment of the requirements of Sally McDonnel Barksdale Honors College.

Oxford
May 2020

Approved by

_____
Advisor: Dr. Davita Watkins

_____
Reader: Dr. Jason Ritchie

_____
Reader: Dr. Randy Wadkins

ACKNOWLEDGEMENTS

First, I want to thank my thesis advisor, Dr. Watkins, for all of her continued support throughout this process. She has been kind and patient with me, and I am so grateful that she provided me with the opportunity to conduct research in her laboratory.

Second, I would like to thank my incredible graduate students, Mahesh and Indika, for all their instruction and support while I worked in the lab. Thank you for your patience with me as I learned how to conduct research. Thank you for all the laughs and all the memories.

I would also like to thank the rest of the Watkins Research Group. In particular, thank you to the entire Janus Dendrimer Team for all your cooperation, assistance, instruction, and feedback. Thank you for always being available when I needed you and for allowing me help with this project.

Thank you to my thesis readers, Dr. Jason Ritchie and Dr. Randy Wadkins of the Chemistry and Biochemistry Department, for agreeing to contribute to this work.

In conclusion, thank you to the Sally McDonnel Barksdale Honors College for providing the opportunity to embark on this endeavor and allowing me to research this topic.

ABSTRACT

Janus dendrimers are amphiphilic macromolecules that have shown promising potential in the biomedical field. Due to their unique structure and properties, these branched block copolymers have the ability to self-assemble into bioinspired spherical nanoaggregates. Because they possess a hydrophobic and hydrophilic moiety, these aggregates show potential as drug delivery systems that can transport both hydrophobic and hydrophilic drugs. However, many of the proposed dendrimer systems suffer from certain weaknesses that hinder their practical usage as clinical treatment options. Some of these shortcomings include specificity, solubility, size, surface charge, and mechanical properties. To combat these problems, we synthesized and characterized a library of PAMAM-fatty acid (PAMAM-FA) hybrid Janus dendrimers that offer solutions to the issues that traditional dendrimers have. These hybrids have a cationic NH_3^+, an anionic COO^-, and a neutral OH surface functionality on the PAMAM moiety, and they have been covalently bonded to fatty acids via click chemistry. These dendrimers show potential in biomedical applications to enhance specificity and to add biological markers to the surface of the PAMAM branches. The nanoparticles in aqueous solution were characterized using microscopy (TEM) and light scattering (DLS), and diameters ranged from 40 to 100 nm. Zeta-potential values ranged from -17.9 mV to +58.7 mV in accordance with the respective surface functionality. TEM images revealed spherical morphologies and showed critical aggregate concentrations (CAC) that ranged from 0.92 to 1.9 μmol/L. The results of our study exhibit strong evidence for the potential use of these hybrids in biomedical applications and clinical settings.

TABLE OF CONTENTS

LIST OF ABBREVIATIONS

DDS	Drug delivery systems
JDs	Janus dendrimers
PAMAM	Polyamidoamine
FA	Fatty acid
Bis-MPA	2,2-bis(hydroxymethyl) propionic acid
TBE	*tert*-butyl ester
THP	tetrahydropyran
BOC	*tert*-butoxycarbonyl
TFA	Trifluoroacetic acid
M_{th}	Theoretical molar mass
M_n	Number average molar mass
M_w	Weight average molar mass
Đ	Dispersity
PDI	Polydispersity index
ζ-potential	Zeta potential
NMR	Nuclear magnetic resonance
GPC	Gel permeation chromatography
DLS	Dynamic light scattering
CAC	Critical aggregation concentration
TEM	Transmission electron microscopy

LIST OF FIGURES AND TABLES

BACKGROUND AND INTRODUCTION

Researchers have been searching for cancer treatments for decades due to the severity and prevalence of the disease. Cancer cells divide uncontrollably, they metastasize to other parts of the body, and they harm surrounding healthy cells by consuming available nutrients. Doctors have been unable to find a singular cure for all cancer types due to the vast complexity and variability among them. In addition, it is difficult to target cancer cells specifically. Chemotherapy and radiation kill cancer cells, but they also kill the surrounding healthy cells. These current methods and medications have advanced, but they still have their shortcomings such as drug loading efficiencies, drug releasing efficiencies, biocompatibility, etc. Due to the lack of selectivity, the many side-effects including hair loss, fatigue, and decreasing immunity often cause additional problems for patients. In addition to selectivity issues, cancer drugs are typically hydrophobic, so it is difficult to transport them via the bloodstream to the target site due to their insolubility.

To resolve these problems of specificity, potency, and solubility, scientists have investigated potential therapies to target cancer sites and minimize the death of healthy cells. One of these therapies include targeted drug delivery using synthetic molecules. Drug delivery systems (DDS) have the potential to revolutionize cancer treatments, and they have other biomedical applications, such as antibiotic therapy[1] and gene transfection[2]. For drug delivery, these vehicles behave as transports to carry drugs to a specific location to be released at a specific time. Scientists have the ability to manage the location specificity via the surface modifications on the DDS. They

can also control the release time and rate through the stability and degradation of the vehicle. These controllable aspects of drug delivery systems drove research scientists to develop different types of DDSs and continue to optimize them.

Researchers have been tirelessly searching for candidates for targeted drug delivery, and there are many vehicles that have been put forth as potential solutions. The ideal DDS is an amphiphilic nanoparticle that can self-assemble into a stable bilayer vesicle to deliver hydrophilic and hydrophobic drugs to a specific target site. Many of the current vehicles that have been synthesized have benefits, but they also have disadvantages. Liposomes are made up of lipids that can form a bilayer with the potential to house hydrophobic and hydrophilic drugs. However, the liposome's lipids do not spontaneously self-assemble. They must be sonicated to take shape, but this method can destroy the phospholipid rendering it an ineffective strategy.[3] Polymeric micelles are also a well-studied potential vehicle. They are amphiphilic, but rather than a bilayer, they form a single layer with the hydrophilic heads on the exterior. Although these are easy to prepare, they have a substantial risk of degrading after they have been administered.[3] The early degradation would cause the drugs to be unleashed too early and kill the healthy cells rather than reaching the target site.

Another popular type of DDS is a dendrimer. In recent years, dendrimers have become one of the primary topics of supramolecular chemistry due to their numerous promising medical applications to solve the previously stated issues. Dendrimers are symmetrical, tree-like macromolecules that can be synthesized in a variety of ways.[4] Some of their benefits include their tunability and controlled synthesis.[5] Traditional dendrimers consist of a central core that allows for a repeating monomer to branch off and continue to repeat in a systematic way.[5] Each additional monomer on the branches constitutes the next "generation" of that dendrimer. The branches end

with an exterior functional group that can be modified to reduce toxicity or attach fluorescent moieties.[5]

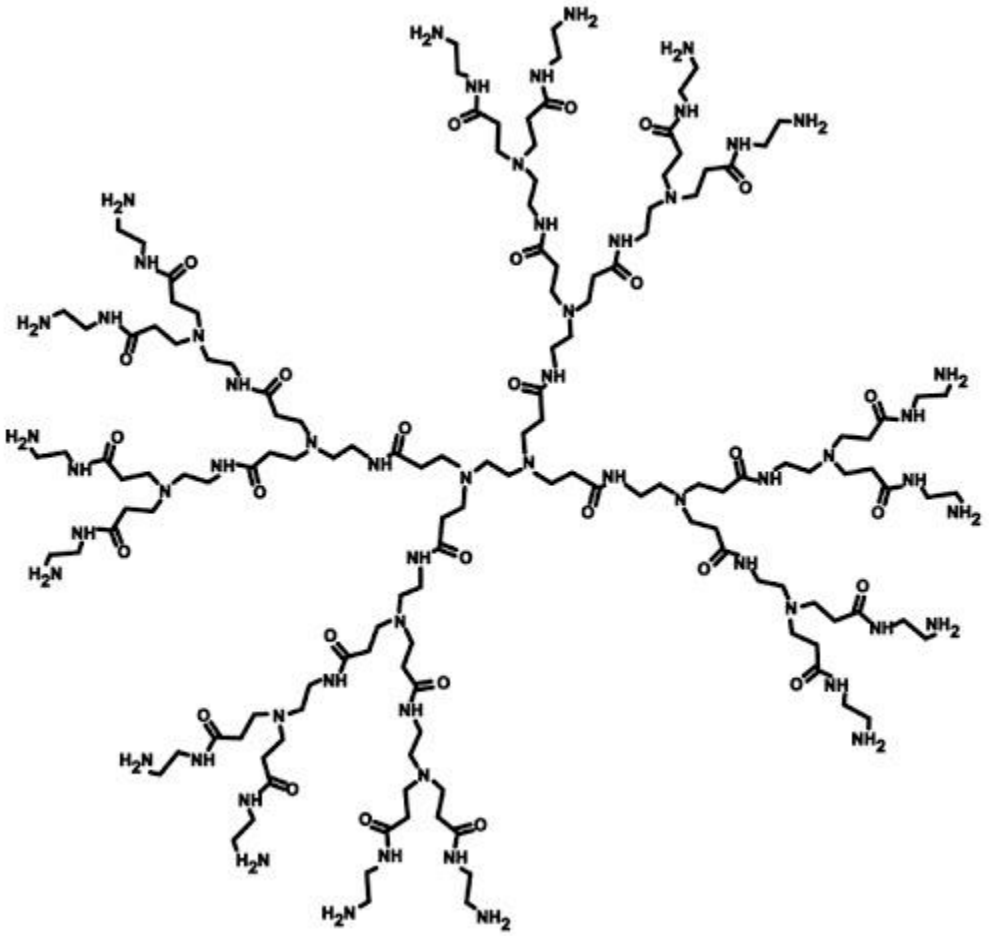

Figure 1.: Traditional G2 PAMAM dendrimer[6]

Dendrimers have been synthesized with a variety of monomers to form various types of macromolecules. One well-studied type is a polyamidoamine (PAMAM) dendrimer which has been studied since it was introduced by Donald A. Tomalia in 1985.[7] Figure 1 shows the structure of a traditional PAMAM dendrimer. It grows symmetrically from the center with repeating methyl acrylate and ethylenediamine segments to form a globular, symmetric macromolecule.

Dendrimers show significant potential for future biomedical applications, but they still have some disadvantages. Some of these include rapid systemic clearance, toxicology issues, solubility, inefficient drug loading, and uncontrolled drug release.[8] To combat these problems, a new class of dendrimers emerged called Janus dendrimers (JDs).

JDs are unique because they lack the symmetric structure of a traditional dendrimer. In contrast, they possess two different dendrons, typically one hydrophilic and hydrophobic dendron, that are connected at the central core. Due to their amphiphilic character, these molecules have the ability to self-assemble into supramolecular nanoaggregates with a variety of structures, including tubes, micelles, and bilayer vesicles.[5,9]

These molecules have been shown to self-assemble into stable nanoaggregates by several researchers. For example, Percec et. al reported that their bilayer vesicles, or dendrimersomes, had much better mechanical properties than both liposomes and polymersomes.[9] Additionally, Peterca et. al reported that their dendrimersomes had mechanical properties that are equivalent to vehicles that are already being used in drug delivery to treat cancer patients.[10]

Their ability to self-assemble into stable aggregates combined with JDs' highly controllable structure allows them to resolve some of the previously stated issues that are associated with traditional dendrimers. Not only are chemists able to manipulate the outer functional groups to enhance selectivity, but they can also manipulate the building blocks of the dendrons to combat cytotoxicity. The self-assembled aggregates have the potential to encapsulate both hydrophobic and hydrophilic drugs, therefore potentially solving the solubility issue. Their stronger mechanical properties could resolve the drug loading and release problems, as well. Due to their amphiphilicity, JDs have the potential to offer solutions to many of the problems that traditional dendrimers could not overcome.

Interestingly, there are different types of JDs that have been suggested by various researchers. Previously, we investigated linear dendritic block copolymers (LDBCs). These macromolecules possess a branched hydrophilic PAMAM moiety and a linear hydrophobic moiety. These molecules were studied by manipulating the weight ratio of hydrophilic to hydrophobic moieties and observing changes in morphology and size. The LDBCs showed promise as they self-assembled to form bilayer vesicles, which is the ideal shape for biomedical applications. In addition, the ideal diameter, 50 to 65 nm, was achieved in this study. However, surface functionalization was not discussed.[11] To further expand on this area of study, our goal is to be able to establish a synthetic route, as well as develop JDs based on PAMAM and FAs as viable candidates, that will capitalize on the current abilities we have established for JDs and minimize the current problems we see in polymeric drug delivery systems.

SCIENTIFIC RATIONALE

There are many different types of polymers and dendrimers in literature that have been used to synthesize JDs. One of the more popular choices is polyamidoamine (PAMAM). We chose PAMAM because it is well studied in literature and still widely used in DDS research. Because we are synthesizing JDs, only about a quarter of a traditional PAMAM dendrimer is being used to create the hydrophilic moiety of our hybrids. It is a highly branched structure, making it more ideal for drug loading, and it has a highly controlled and systematic synthesis. It also can be terminally functionalized with various end groups which allows for further potential biomedical applications and decreased toxicity.[12] In addition, PAMAM is made up of repeating methyl acrylate and ethylenediamine segments that form amide bonds. These bonds resemble the structure of biological proteins that also possess repeating amide bonds.[2,12] These polypeptide-like bonds cause

this highly branched structure to take on some properties of proteins, sometimes being referred to as "artificial proteins," and they have been found to have low mammalian toxicity.[2]

While PAMAM is used for the hydrophilic portion, the hydrophobic portion is made up of fatty acids (Figure 2). These molecules are a more familiar term and are a well understood in biology and medicine. Biologists have known for a long time about their roles in cell membranes and energy storage in humans.[13] Because they are native to the human body, they are biocompatible and biodegradable, making them a logical candidate to use in the synthesis of delivery vehicles.[14] Like PAMAM, there are also several studies that have been recorded in the literature about their influence in drug delivery.[4,14,15] For example, Silvia Hernández-Ainsa et. al ionically functionalized their PAMAM G2 dendrimers with fatty acids of varying sizes to determine the effects on the self-assembling properties of their vehicles.[15] Our study also employed the use of fatty acids to observe their effects on the self-assembling properties, however, our fatty acids are covalently bonded rather than ionically bonded. Fatty acids can be attached covalently via esterification to 2,2-bis(hydroxymethyl) propionic acid (bis-MPA) based dendrimers.[4] A bis-MPA based dendrimer, which is a well-studied type of delivery system, was employed in our vehicle because using a covalent bond yields a more stable molecule that does not rely on the number of positive and negative ions.[4,16] Additionally, bis-MPA dendrimers are polyesters making them biodegradable and biocompatible, and their terminal alcohol groups allow it to be protected, deprotected, and esterified with fatty acids.[16] Another advantage of the bis-MPA core is the ability to manipulate the number of terminal alcohol groups, similar to manipulating the number of PAMAM terminal groups. With this high level of control, we can do further studies on the impact of varying ratios of fatty acids by growing or condensing the core to attach more fatty acids.

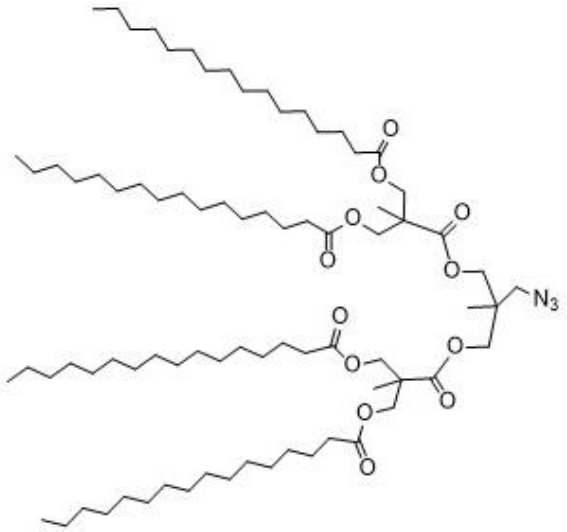

Figure 2. Fatty acid portion of the hybrid

Herein, we introduce the novel PAMAM-Bis-MPA-4-Fatty Acid hybrid dendrimer with a PAMAM-G3 moiety and a Bis-MPA based moiety esterified with 4 fatty acid chains (Figure 3). As previously stated, PAMAM was a logical choice for the hydrophilic portion due to the extensive research that has already been conducted by numerous researchers.[8,9,10] For this work, we chose to use generation 3 (G3) for our hybrids. Studies have shown that larger generations of PAMAM suffer from steric crowding due to excessive branching,[12] while smaller generations are too flexible leading to cargo leaking.[17]

This macromolecule has been successfully synthesized with three different end groups. These include a carboxylic acid which becomes anionic in PBS buffer (COO^-) at pH = 7.4, a neutral alcohol (OH), and a cationic amine (NH_3^+) in Milli Q water at pH = 7.0. For the lipophilic portion, we introduced the fatty acid side chains on an azide-bis-MPA-4-OH dendron. They have the potential to increase the mechanical properties and, therefore, the strength and stability of the nanocarrier due to stronger hydrophobic interactions. The two segments were joined via click

chemistry. Upon deprotection, the dendrimers become amphiphilic and have the ability to self-assemble into nanoparticles.

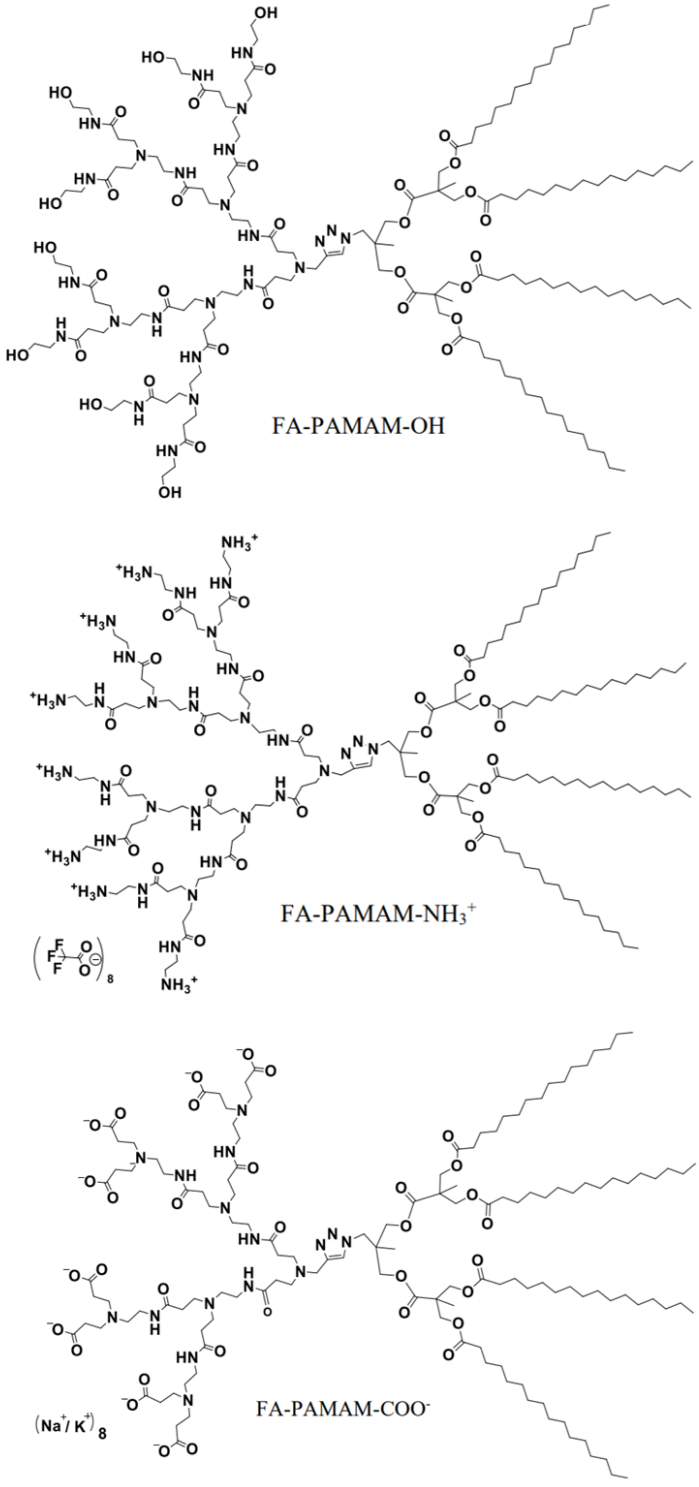

Figure 3. The three PAMAM-FA hybrids

The design and synthesis of these dendrimers are unique and novel in that they can be modified with a variety of end groups. The exterior groups on the PAMAM moiety include a carboxylate, alcohol, and an amine. Each of these groups has a protecting group that can be removed in the final step of the synthesis. These protecting groups are *tert*-butyl ester (TBE), tetrahydropyran (THP), and *tert*-butoxycarbonyl (BOC). The TBE end group protects the carboxylic acid, THP protects the neutral alcohol, and BOC protects the amine. These end groups have exhibited different benefits in various studies. For example, cationic terminal amines have shown increased uptake,[18] anionic nanoparticles have shown higher circulation time in the bloodstream,[19] and neutral nanoparticles have been reported as a successful delivery system without appreciable toxicity.[20]

The three different end groups on our vehicles also provide another benefit for potential use. The terminal carboxylate, amine, and alcohol can be the starting materials to add a variety of biochemical molecules to the exterior groups on the PAMAM portion of the vehicle. This high level of specificity with respect to the outer groups is particularly valuable for cancer treatments. Different types of cancerous cells have different properties, which leads to the difficulty in synthesizing a single cure. However, our JDs have the potential to be a starting molecule from which more specific vehicles could be synthesized. In other words, a JD's hydrophilic terminal end groups could be modified with biochemical markers to find specific types of cancer cells, thus further increasing the specificity of the vehicles.

Overall, our new PAMAM-fatty acid hybrid JD shows promising potential in combating many of the numerous issues that have hindered the advancement of specific cancer treatments including toxicity to healthy cells, potency, solubility, and stability.

RESULTS AND DISCUSSION

DESIGN STRATEGY

PAMAM

Our PAMAM-fatty acid hybrid contains two dendritic moieties joined together via click chemistry. PAMAM makes up the hydrophilic portion, and the fatty acids are hydrophobic (Figure 4). PAMAM is synthesized with alternating Michael additions and amidations using methyl acrylate and ethylenediamine to create a branched polymer. Because of the stepwise repetition, PAMAM can be synthesized to form varying sizes with different amounts of branching.

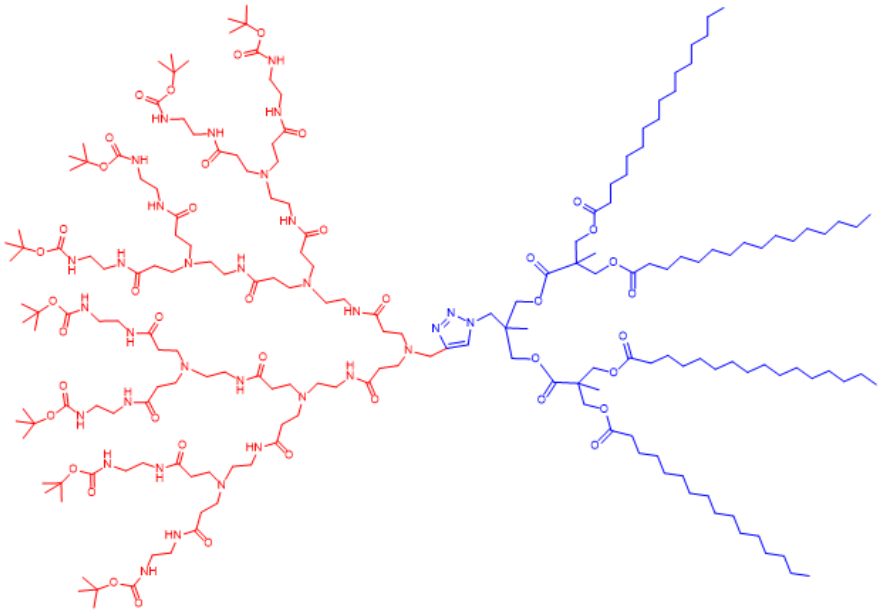

Figure 4. Example of the hybrid showing the hydrophilic (red) and hydrophobic (blue) moieties.

PAMAM is also ideal for terminal functionalization. We have successfully functionalized the terminal ends with three different groups (Figure 5). The functionalization of the PAMAM surface is important to the toxicity of the vehicle.[2,12] The repeating amide segments mimic the makeup of biological molecules,[2] however, exposed cationic amine groups are toxic to human cells.[21] The large positive charge rips the anionic cell membrane of human cells apart, therefore it is harmful to healthy cells.[21] However, it is beneficial to have a small overall positive charge to encourage interaction between the DDS and cells.

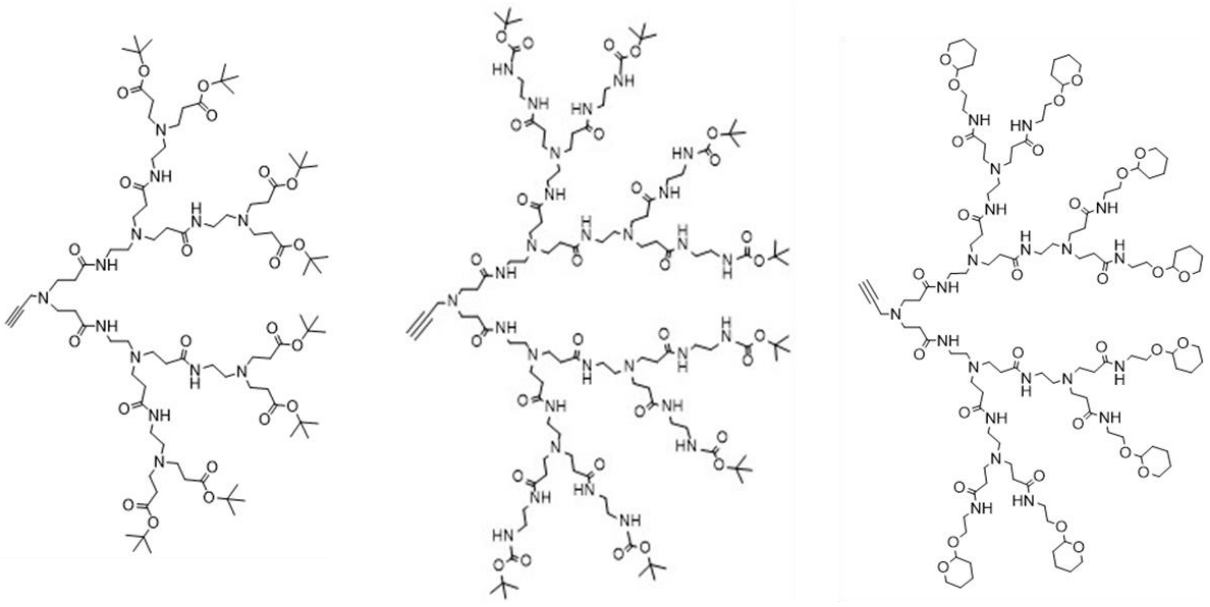

PAMAM-TBE PAMAM-BOC PAMAM-THP

Figure 5. The three PAMAM moieties with TBE, BOC, and THP protection groups

The various end groups also allow the potential for other biochemical groups to be covalently bonded to the ends of the PAMAM moiety. This could lead to advancements in increasing specificity. For example, some forms of cancer overexpress biotin receptors on the cell surface.[22] By attaching biotin to the ends of PAMAM, the DDSs will be more likely to dock with the cancer cells and unload the drugs at that specific location.[22] The different biomarkers can be

chemically attached with a variety of reactions including acylation, Michael addition, and amidation.[23]

The PAMAM dendron was synthesized using the divergent method. This method uses the core as the starting point and grows the branches from this central molecule.[2] The core functional group for PAMAM is propargyl amine. The first half-generation of PAMAM is formed via a Michael addition with the core and methyl acrylate. This step is followed by a nucleophilic amidation with ethylenediamine to yield the first full generation. These steps are repeated to grow the PAMAM dendron until generation 3 (Scheme S4). The amine-terminated generation 3 dendron was treated with di-tert-butyl dicarbonate in methanol to obtain P-PAMAM-G3-BOC with 92% yield. PAMAM generation 2.0 was treated with tertbutyl acrylate in methanol to obtain P-PAMAM-G3-TBE with a 90% yield. PAMAM generation 2.5 was treated with ((tetrahydro-2H-pyran-2-yl)oxy)methanamine in methanol to obtain P-PAMAM-G3-THP with 81% yield (Figure 6).

TBE - *tert*-butyl ester THP – tetrahydropyran BOC- *tert*-butoxycarbonyl

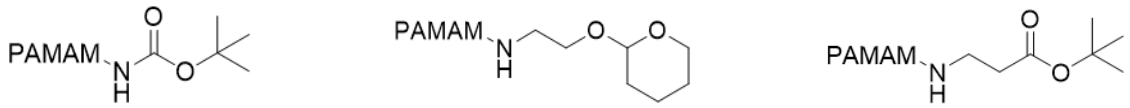

Figure 6. End groups on the PAMAM moiety

FATTY ACIDS

The lipophilic fatty acid chains were chosen for their well-studied nature in human biology. Fatty acids are used in the body to make up cell membranes, store energy, and make up other macromolecules in the body. The biocompatibility and biodegradability make fatty acids a good choice for creating nontoxic drug vehicles. Additionally, the fatty acid chains are responsible for

the hydrophobic interactions that are the driving force for the self-assembly of the nanocarriers. These are the same forces that create the bilayer of cell membranes in the human body, and therefore show promise in increasing the stability and strength of DDSs.

The fatty acid portion contains an azide-bis-MPA-4 core with fatty acids esterified to the four terminal alcohol groups. We chose fatty acids because of their potential enhancement of mechanical properties of our DDSs. Fatty acids exhibit strong hydrophobic interactions which have the potential to strengthen the stability of the vehicle and prevent early release of the drug. In addition, fatty acids are a well-understood bio-molecule in the human body, thus the fatty acid moiety is biocompatible.

The bis-MPA core is composed of polyesters, and it is first synthesized with a substitution scheme to substitute an alcohol group with an azide to later perform the click reaction. Next, the resulting A-MPA-2-OH is esterified with the bis-MPA monomer, followed by an acetal deprotection to yield A-MPA-4-OH. The polymer's terminal alcohol groups are esterified to form the final A-bis-MPA-4-FA hydrophobic moiety (Scheme S2).

The hydrophobic, fatty acid moiety was also synthesized using the divergent method. The core of the lipophilic dendron is an azide group, and the branches are grown using a bMPA monomer. Using 1,1'-carbonyldiimidazole (CDI) to activate the carbonyl group and cesium fluoride (CsF) as a catalyst, a Malkoch esterification yielded A-bis-MPA-OH-4. The 4 alcohol groups were esterified with palmitoyl chloride to afford A-bis-MPA-FA-4 with a 91% yield (Scheme S2). Presence of the azide group was confirmed by the FTIR using stretching vibrations at 2102 cm^{-1} (Figure 7).

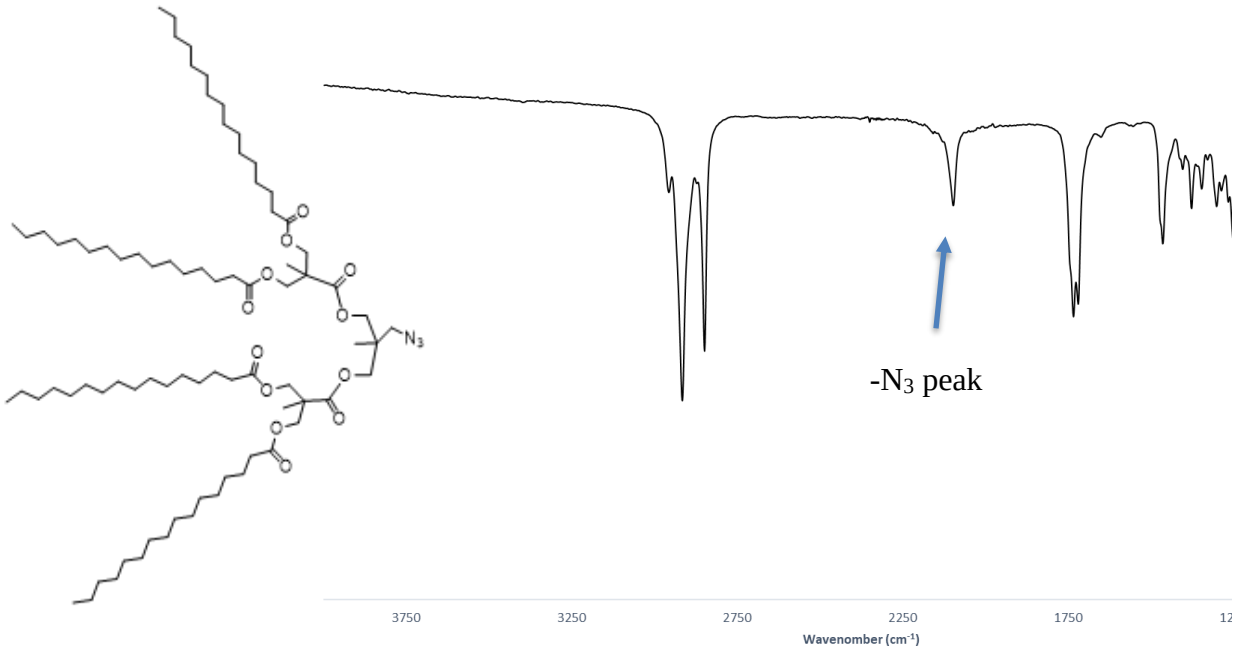

Figure 7. FTIR spectra for A-MPA-4-FA (10)

PAMAM-FA

After synthesizing both half-dendrons separately, they were linked via click chemistry. We synthesized the core of the 2 dendrons to have a propargyl amine and an azide to covalently bind them together using copper(I)-catalyzed azide-alkyne cycloaddition (CuAAC) (Figure 8). The reaction was carried out with the hydrophobic dendron in excess to increase product yields. It also is easier to separate the final JD from the hydrophobic portion due to the greater difference in molar mass. This difference allows for separation of the two molecules via size exclusion chromatography, a method that is somewhat different from previous methods described in literature. Additionally, this method provided good yields of all three JDs (79-86%). After purifying the product, the protecting groups on the terminal ends of the PAMAM moiety, TBE, BOC, and THP, are removed using trifluoroacetic acid (TFA). The deprotection yields the final Janus dendrimers: FA-PAMAM-NH_3^+, FA-PAMAM-COO^- and FA-PAMAM-OH.

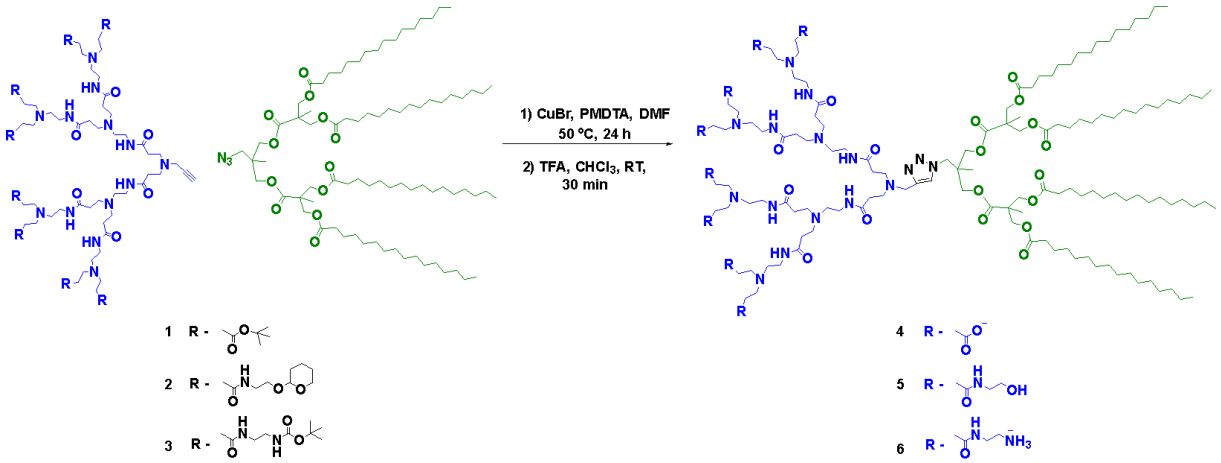

Figure 8. Synthetic route for amphiphilic JDs

^{1}H and ^{13}C NMR spectroscopy were used to monitor the reactions and to confirm the intermediate products (Figure S1-S30). Additionally, ^{1}H and ^{13}C NMR and GPC were used to characterize the final synthetic 'click' products. FA-PAMAM-BOC is used to demonstrate the characterization results of the compounds. The center triazole ring that forms during the click reaction creates a new peak in the ^{1}H NMR spectrum at 8.06 ppm that corresponds to H-3 (Figure S24-S23). Additionally, the ^{13}C NMR spectrum exhibits two new peaks at 144 and 125 ppm that correspond to C-1 and C-2, respectively, of the triazole ring to further confirm the completion of the click reaction (Figure 9). The protons at the α positions of the triazole ring, H-1, correspond to the hydrophilic PAMAM moiety, and their peaks shift downfield from 3.62 to 4.40 ppm relative to the starting PAMAM dendron (Figure S23). Similarly, the protons at the α positions of the triazole ring, H-4, correspond to the hydrophobic fatty acid moiety, and their peaks shift downfield from 3.32 to 4.29 relative to the starting fatty acid dendron (Figure S23). The peaks that correspond to PAMAM (2.19-3.69 ppm) and bMPA fatty acid (1.57, 5.15 ppm) remained unchanged, and the integrations for each peak accurately reflect both hydrophilic and hydrophobic moieties (Figure S23).

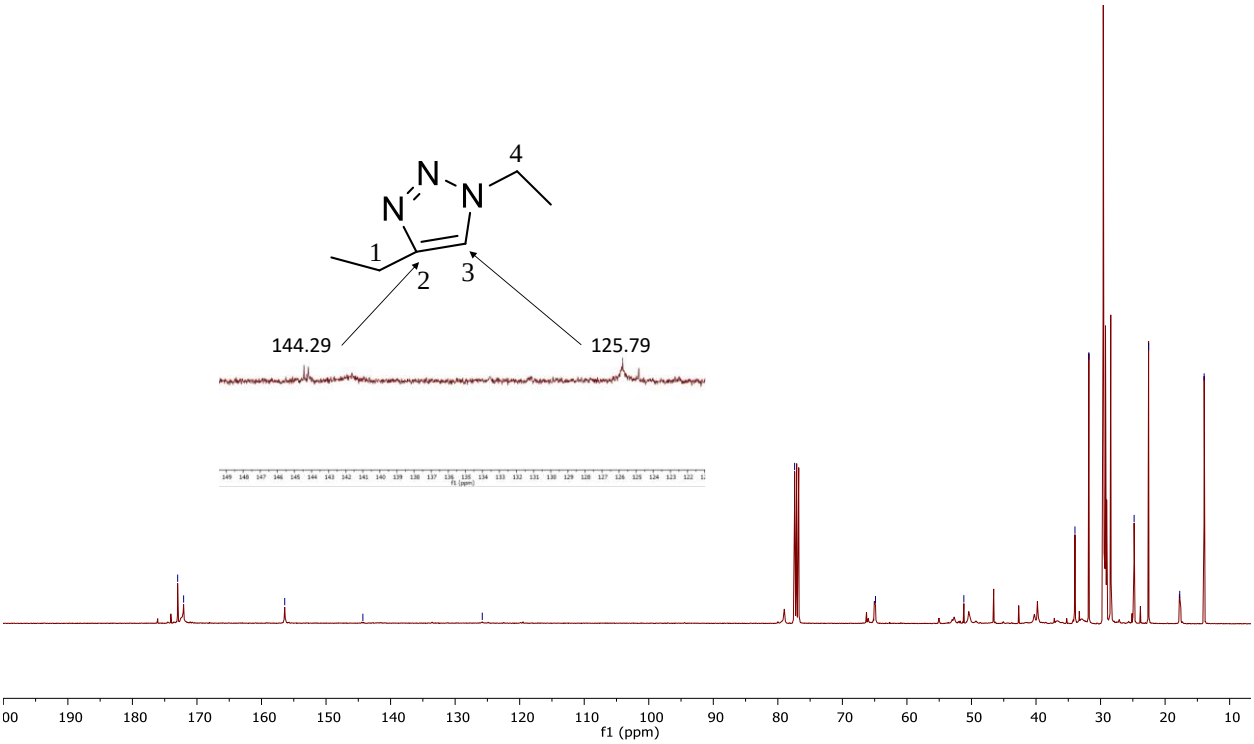

Figure 9. ^{13}C NMR spectrum for FA-PAMAM-BOC in $CDCl_3$ recorded at 400 MHz

Further characterization of the JDs was done using GPC (Table 1). In particular, GPC was used to determine the monodispersity of the final product and confirm that there were no free, unreacted dendrons that remained in solution after the CuAAC coupling process. GPC was run using protected JDs due to their solubility in THF, and each compound's results revealed a single peak on the GPC chromatogram indicating that there is one macromolecule in solution and no free, unreacted dendrons (Fig S31-S33). The shoulders that appear in the GPC data is due to the hydrophilic branching of the JDs which interacts with the hydrophobic column and affects its elution rate.[11] In addition, the retention peak of the starting material does not correspond to the shoulder on the final product, thus our data shows that we have no free dendrons that had not reacted during the CuAAC process.

TABLE 1. Molecular Weight Characterization of JDs by GPC with THF as the elution solvent; chromatographs shown in the supporting information figures.

Sample	**M_{th} g mol^{-1}**	**M_n g mol^{-1}**	**M_w g mol^{-1}**	Đ[a]
FA-PAMAM-G3-BOC	3785	3625	3801	1.05
FA-PAMAM-G3-TBE	3096	3118	3289	1.06
FA-PAMAM-G3-THP	3665	3716	3781	1.02

[a]M_{th}, M_n, M_w, Đ denote theoretical molar mass, number average molar mass, weight average molar mass and dispersity, respectively. In GPC, the dispersity, Đ, refers to the distribution of the molecular weight of a JD. It is measured as M_w/M_n, and an ideal value is 1.0.[24]

SELF-ASSEMBLY AND MORPHOLOGY

TABLE 2. CAC values, the average hydrodynamic diameter of the dendritic aggregates by TEM and DLS (in number and intensity), and surface charge.

Sample	CAC (μmol L^{-1})	D_h(nm)		PDI[a]	ζ-potential (mV)
		Number	Intensity		
FA-PAMAM-G3-NH_3^+	1.9 ± 0.2	57.8 ± 16.7	103.7 ± 40.3	0.191	56.1 ± 6.5
FA-PAMAM-G3-OH	0.92 ± 0.2	41.0 ± 9.0	53.3 ± 12.4 308.2 ± 85.1	0.469	8.5 ± 1.6
FA-PAMAM-G3-COO^-	0.92 ± 0.2	93.1 ± 15.9	102.2 ± 14.1	0.882	-17.9 ± 2.6

[a]In DLS, the dispersity, or PDI, refers to the distribution of the different sizes of the aggregates. It is measured as the square of the standard deviation divided by the mean, and the ideal value is 0.1.[24]

Self-assembly of the three different JDs was accomplished using the nanoprecipitation method.[25,26] Water was used for the formation of FA-PAMAM-NH_3^+ aggregates, and a PBS buffer was used for the FA-PAMAM-COO^- and FA-PAMAM-OH aggregates. After the nanoparticles assembled, we measured the critical aggregation concentration (CAC) (Table 2, Figure S34-S35). CAC values correlate to the concentration that determines if the JDs will remain self-assembled. If the concentration is above the CAC, they will form the vehicle. Below this concentration, the vehicle will not form. The CAC values are measured by using pyrene as a solvatochromic fluorophore. Pyrene is a hydrophobic molecule that exhibits different fluorescent profiles depending on if it is in water or in a lipophilic medium. If the JDs self-assemble, then pyrene will aggregate in the lipophilic layer of the vehicle, and the appropriate fluorescent profile will be detected. As a result, the CAC values can be measured. The CAC values can provide an indication of the stability of the nanoparticle. A lower CAC value indicates a more stable vehicle relative to a higher CAC. It is critical for the CAC to be relatively low due to the vehicles inevitable dilution

when it enters the bloodstream. As shown in Table 2, the CAC ranged from 0.92 to 1.9 μmol/L. These values are similar to the CAC values of other vehicles that are potential candidates for biomedical applications.[27,28]

The CAC values for these macromolecules are all relatively low, but they do vary slightly based on the surface charge. Positively charged FA-PAMAM-NH_3^+ has the largest CAC value (1.9 μmol/L), and anionic FA-PAMAM-COO^- and FA-PAMAM-OH had the smaller value (0.92 μmol/L). These results suggest that the anionic and neutral JDs form more stable nanoparticles than the cationic JD.

The corresponding diameters for the different JD aggregates were determined using dynamic light scattering (DLS) (Table 2, Figure S31-S33). Here we include the number and intensity value. The number diameter represents the diameter of the majority of the aggregates formed. The intensity diameter is the average diameter of all the aggregates, but the value favors the largest aggregates formed. Our research primarily focuses on the number diameter. Anionic JDs have a larger particle size with the number average radii 93.1 nm, intensity average radii 102.2 nm with 0.882 PDI. For the neutral JD, number average radii 41.0 nm, intensity average DLS data gave two distributions, small hydrodynamic diameters (53.3 nm), and larger hydrodynamic diameter (308.2 nm) with 0.469 PDI (Figure S33). Cationic JD shows similar particle size to neutral JD with number average radii 57.8 nm, intensity average radii 103.7 nm with 0.191 PDI. Based on the PDI value, cationic JDs and neutral JDs show a narrow size distribution where PDI values range from 0.1 to 0.5, and anionic JDs show a broad distribution with a PDI value greater than 0.5. All particle sizes are below 200 nm, which indicates that they have the potential to escape physiological barriers such as the enhanced permeability and retention effect. They also have a

high potential for prolonged circulation and reduced filtration by the liver and spleen. Therefore, these nanoparticles can be developed as drug gene delivery agents and cancer therapy agents.[29]

Because DLS data is reliant on the spherical shape of the nanoparticle, it is crucial to use microscopic examination to determine the morphology. Cryo-TEM reveals the dendrimers' behavior as predicted in aqueous solutions, and it exhibits the different morphologies of the self-assembled JD aggregates (Figure 10). All of the images show that the JDs form spherical nanoparticles when they self-assemble, thus validating the DLS data. The images of FA-PAMAM-G3-NH_3^+ (Figure 10a) showed spherical aggregates with an average particle size of 55.6 nm. The images correlated with the DLS data that reported a single average radius of 57.8 nm. FA-PAMAM-G3-OH (Figure 10b) formed spherical aggregates that were isolated, which had an average particle size of 47.5 nm, and they formed clusters of nanoparticle aggregates. This explained why the DLS data showed two average radii of 53.2 nm and 308.2 nm. Because DLS is not designed to measure multimodal particle size distributions, the signal of the smaller particle is much weaker. Finally, FA-PAMAM-G3-COO^- (Figure 10c) assembled into spherical aggregates with an average particle size of 104.8 nm. This value corresponds to the average radii of 93.1 nm that was measured by DLS. In conclusion, the FA-PAMAM-OH JDs formed more aggregates relative to the cationic and anionic JDs which could be due to the neutral surface charge. Unlike the charged JDs, the neutral JD does not experience charge separation between the nanoparticles. This contributes to the formation of more aggregates with the support of hydrogen bonding between the terminal alcohol groups.

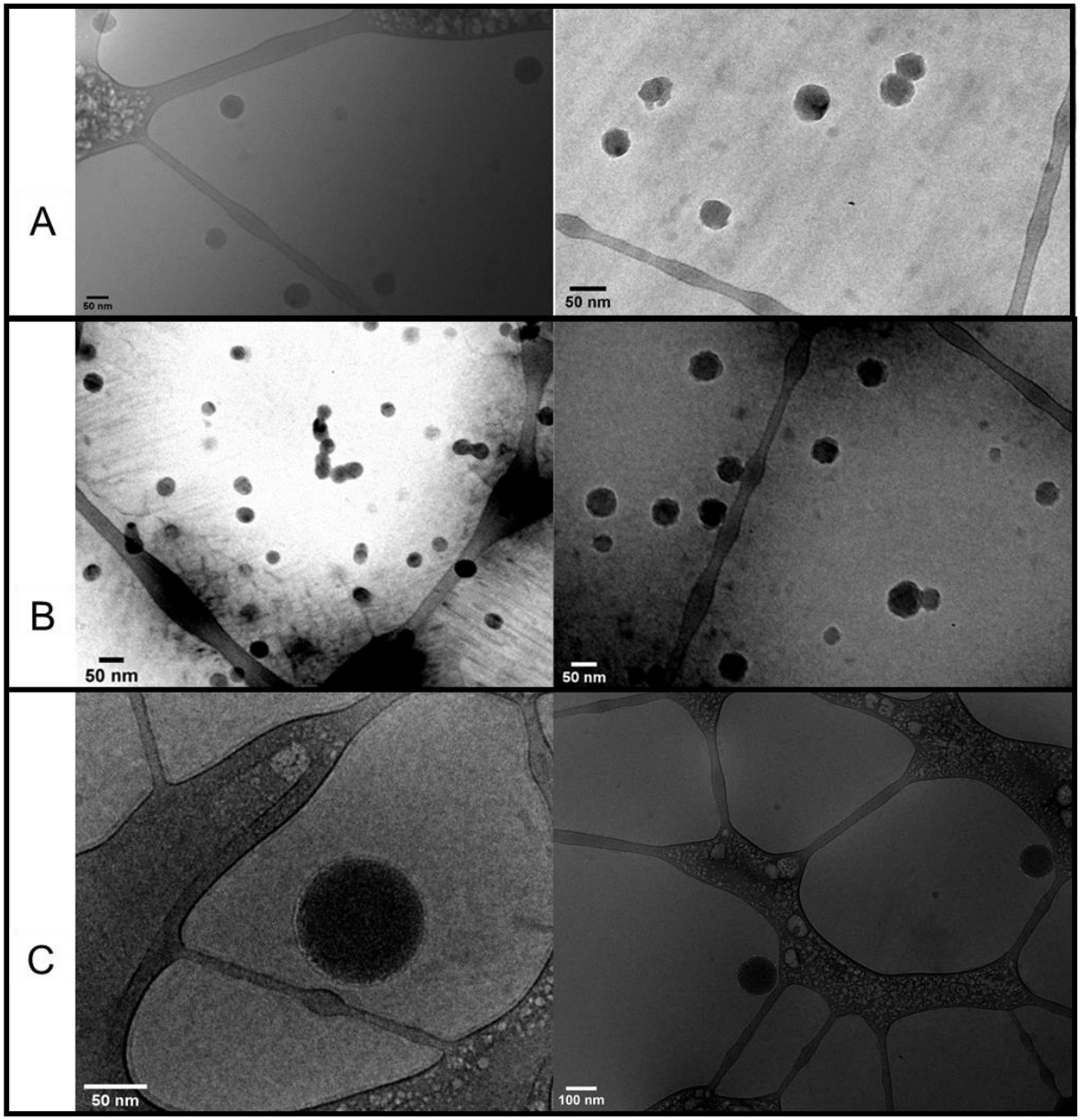

Figure 10. Cryo-TEM images with utilizing uranyl formate as a contrast agent for (A) FA-PAMAM-G3-NH_3^+, (B) FA-PAMAM-G3-OH and (C) FA-PAMAM-G3-COO^-.

The zeta potentials were also studied to determine the surface charge of the aggregates formed from the amphiphilic JDs (Table 2). FA-PAMAM-G3-NH_3^+ had a surface charge of 56.1 ± 6.5 mV in Milli Q water at pH 7.0. FA-PAMAM-G3-COO^- had a surface charge of -17.9 ± 2.6 mV at pH 7.4 in PBS buffer. Lastly, FA-PAMAM-G3-OH had a charge of 8.5 ± 1.6 mV at pH 7.4

in PBS solution. The resulting zeta potential values correspond to the expected values of each JD's respective terminal charge. In literature, particles with surface charges below 15 mV displayed the ideal properties such as decreased macrophage uptake,[30] higher tumor retention, and longer circulation time.[31] This indicates that our neutral JDs have a greater potential to exhibit these properties, as well. Also, the ideal surface charge depends on factors such as cell type, cellular uptake mechanism, and intracellular localization of nanoparticles.[18,32] Therefore, the cationic and anionic JDs have the potential to be useful for other applications in which a more positive or more negative charge is needed.

CONCLUSION

In this study, we successfully synthesized and characterized cationic, anionic, and neutral amphiphilic PAMAM-fatty acid Janus dendrimers. TEM and DLS analysis indicate the size of spherical nanoparticles ranging from 40 to 100 nm with zeta-potential values ranging from -17.9 to +58.7 mV concerning the terminal functional group. Further, these systems exhibited spherical aggregates with critical aggregate concentrations ranging from 0.92 to 1.9 μmol/L. Of these three, the neutral FA-PAMAM-OH had a low CAC value, and the zeta potential revealed an ideal surface charge for future biomedical applications. This study showed that Janus dendrimers with neutral surface charges exhibit characteristics that indicate their strong candidacy as potential drug delivery systems. Further studies regarding drug loading capacity, pH studies, and cytotoxicity still need to be conducted. Additional studies regarding the optimization of the vehicle could also be conducted to determine the best hydrophilic to hydrophobic ratio to achieve ideal mechanical properties. Finally, studies to investigate a synthetic route for JDs with two surface functionalities would be beneficial for manipulating the surface charge. Although there is still work to be done in the realm of cancer treatment, our results revealed new insights for progress in drug delivery system research.

SYNTHESIS SCHEMES

SYNTHETIC DETAILS

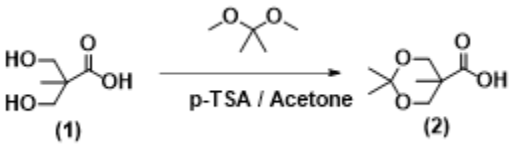

Scheme S1. Synthesis of 2,2,5-trimethyl-1,3-dioxane-5-carboxylic acid

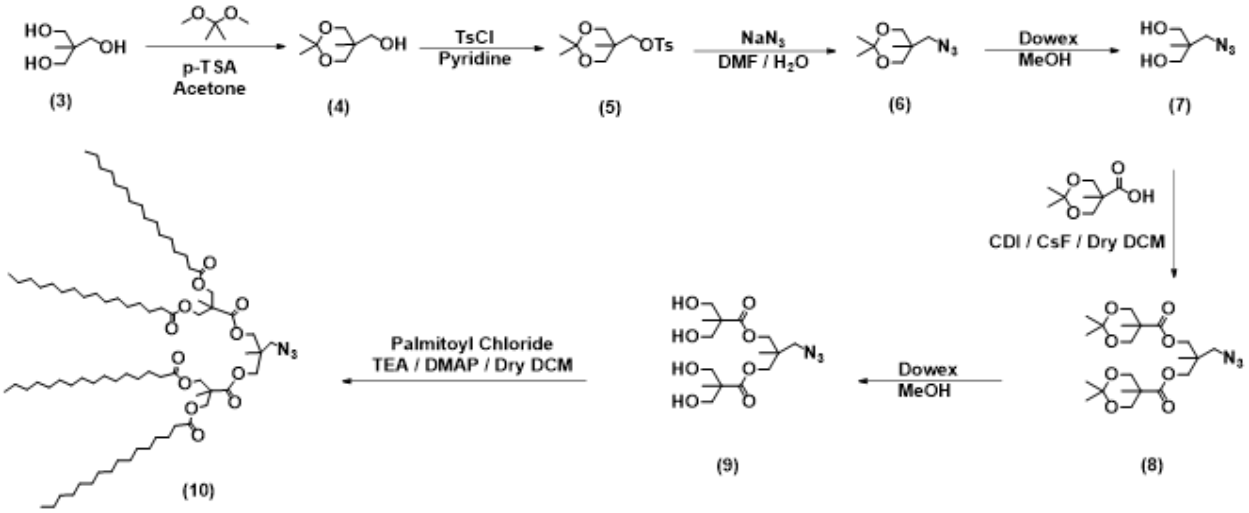

Scheme S2. Synthesis of hydrophobic dendron

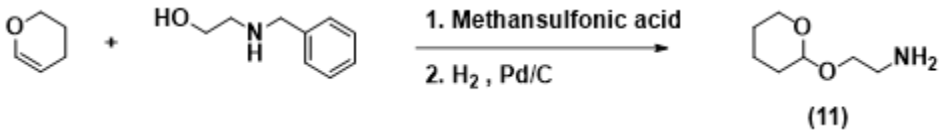

Scheme S3. Synthesis of ((tetrahydro-2H-pyran-2-yl)oxy)methanamine

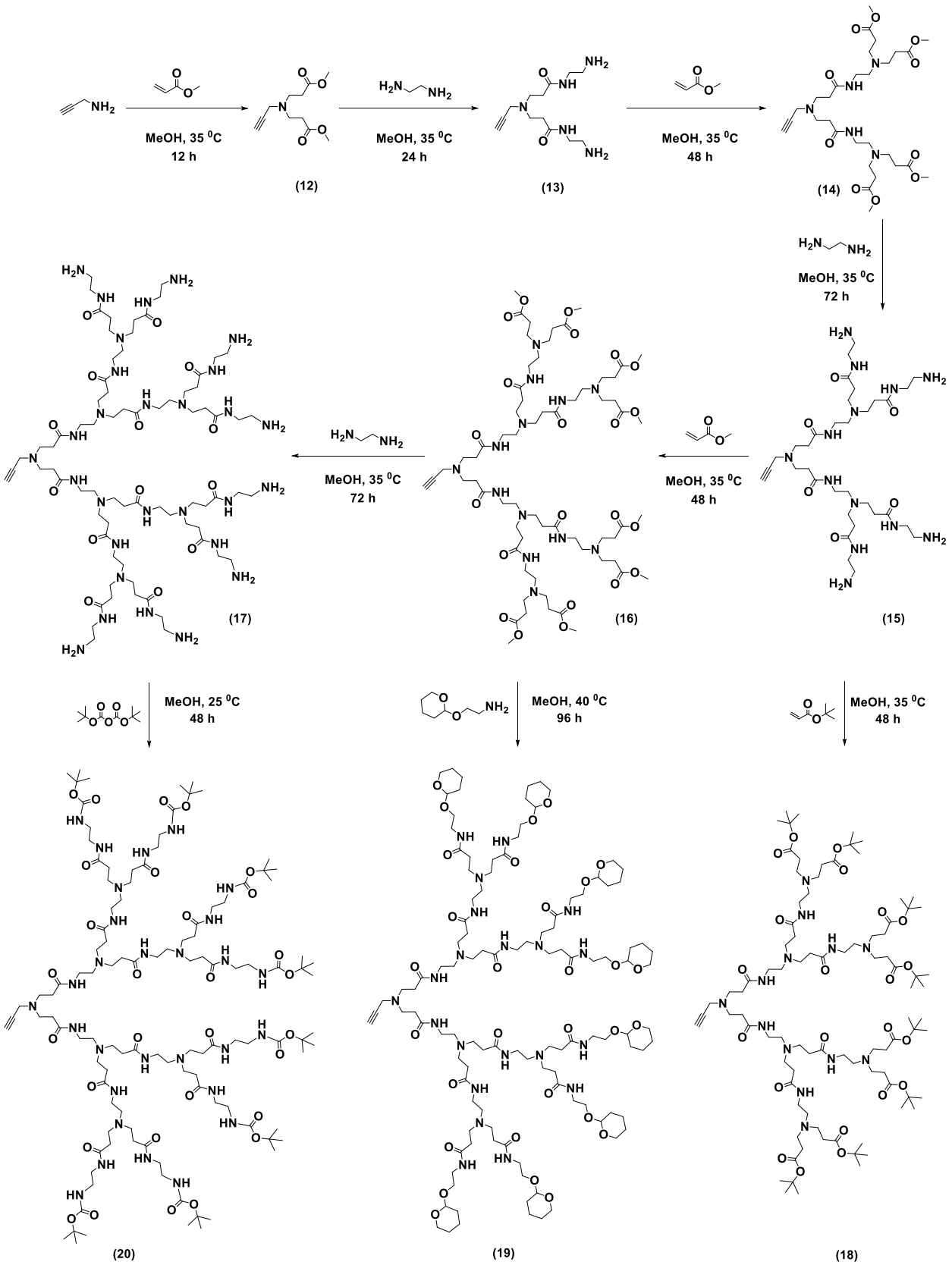

Scheme S4. Synthesis of hydrophilic dendron

Reported below are the full synthetic details for the preparation of monomers, dendrons, and amphiphilic Janus dendrimers

2,2,5-trimethyl-1,3-dioxane-5-carboxylic acid (2)

This procedure was adapted from previously reported procedures.[1] To the stirred solution of 3-hydroxy-2-(hydroxymethyl)-2-methylpropanoic acid (100.06 g, 0.750 mol) in 500 mL of acetone, 2,2-dimethoxypropane (DMP) (116.47 g, 1.12 mol) and p-toluenesulfonic acid (PTSA) (7.10 g, 37.2 mmol) were added under room temperature. After the completion of the addition, the reaction mixture was stirred 5 h. Then it was filtered through an amberlyst column and the solvent was evaporated at room temperature. The residue was recrystallized using CH_2Cl_2 to give (2) white crystals with 92% yield (120.20 g). ^{1}H NMR (500 MHz, $CDCl_3$) δ 4.27 – 4.17 (m, 2H), 3.76 – 3.66 (m, 2H), 1.55 – 1.39 (m, 6H), 1.23 (d, J = 2.8 Hz, 3H).

(2,2,5-trimethyl-1,3-dioxan-5-yl)methanol (4)

This procedure was adapted from previously reported procedures.[2] To the stirred solution of 2-(hydroxymethyl)-2-methylpropane-1,3-diol (10.10 g, 84.0 mmol) in 50 mL of acetone, 2,2-dimethoxypropane (DMP) (13.14 g, 0.126 mol) and PTSA (0.79 g, 0. 4.14 mmol) were added under room temperature. After the completion of the addition, the reaction mixture was stirred 4 h. Then it was filtered through an amberlyst column and the solvent was evaporated, and the residue was put under 60 ^{o}C and full vacuum for 2 h. Then it was put under vacuum overnight to give (4) as a colourless liquid with 96% yield (12.91 g). ^{1}H NMR (500 MHz, $CDCl_3$) δ 3.67 (d, *J* = 5.3 Hz, 4H), 3.60 (d, *J* = 11.8 Hz, 2H), 1.44 (s, 3H), 1.40 (s, 3H), 0.83 (s, 3H).

(2,2,5-trimethyl-1,3-dioxan-5-yl)methyl 4-methylbenzenesulfonate (5)

This procedure was adapted from previously reported procedures.[2] Compound (4) (10.89 g, 68.0 mmol) was dissolved in 34 ml of pyridine and it was added dropwise to the stirred solution of p-toluenesulfonyl chloride (35.70 g, 0.187 mol) in 48 mL of pyridine at 0 ^{o}C under nitrogen. After the complete addition, reaction mixture was stirred 48 h at room temperature. Then the reaction mixture was added dropwise to 100 ml of 40% ammonium chloride solution at 0 ^{o}C. After complete addition, it was allowed to stir at room temperature for 2 h. Then it was filtered and washed with DI water until the pyridine smell was gone. Then the residue was dissolved in 25 ml of DCM and extracted with half saturated ammonium chloride and saturated NaCl solution. Yellow DCM solution was dried with anhydrous sodium sulfate. Then the solvent was evaporated, and the residue was placed under full vacuum for 12 h to give (5) as a yellow solid with 89% yield (19.02 g). ^{1}H NMR (500 MHz, $CDCl_3$) δ 7.86 – 7.79 (m, 2H), 7.38 (d, *J* = 7.6 Hz, 2H), 4.11 (s, 2H), 3.58 (s, 4H), 2.47 (s, 3H), 1.39 (d, *J* = 4.8 Hz, 3H), 1.25 (d, *J* = 4.7 Hz, 3H), 0.84 (s, 3H).

5-(azidomethyl)-2,2,5-trimethyl-1,3-dioxane (6)

This procedure was adapted from previously reported procedures.[2] Compound 5 (14.60 g, 46.4 mmol), NaN_3 (12.07 g, 186 mmol), water (10 mL), and DMF (80 mL) were stirred at 110 °C for 48 h under reflux. The mixture was poured into 150 ml water and extracted four times with Et_2O (4 × 200 mL). The organic phase was dried over anhydrous $MgSO_4$ and the solvent was removed under reduced pressure. The residue was purified by column chromatography with silica gel (100 g) and ethyl acetate/n-hexane (1:4) to give 7.48 g of a colourless liquid with an 87% yield. ^{1}H NMR (500 MHz, $CDCl_3$) δ 3.58 (d, J = 2.8 Hz, 4H), 3.51 (s, 2H), 1.40 (d, J = 13.8 Hz, 6H), 0.81 (d, J = 1.1 Hz, 3H).

2-(azidomethyl)-2-methylpropane-1,3-diol (7)

This procedure was adapted from previously reported procedures.[4] Compound (6) (7.05 g, 40.2 mmol) was dissolved in 35 ml of methanol. 7.00 g of a Dowex, H^+ resin was added, and the reaction mixture was stirred for 12 h at 50 ^{o}C. When the reaction was complete the Dowex, H+ resin was filtered off in a vacuum filter under a low vacuum and carefully washed with methanol. The methanol was evaporated to give 5.41 g of white crystals with a 93% yield. ^{1}H NMR (400 MHz, $CDCl_3$) δ 3.73 – 3.58 (m, 4H), 3.56 – 3.43 (m, 2H), 2.19 (s, 2H), 0.89 (d, J = 2.0 Hz, 3H).

A-MPA-4-AC (8)

This procedure was adapted from previously reported procedures.[3] Compound 2 (6.48 g, 37.2 mmol), 1,1'-carbonyldiimidazole (CDI) (9.05 g, 55.8 mmol) were dissolved in 30 ml of ethyl acetate and it was stirred 1 h at 50 °C. CsF (0.75 g, 4.93 mmol), Compound (7) (1.80 g, 12.4 mmol) were dissolved in 10 ml of ethyl acetate separately and it was slowly added to the reaction mixture under nitrogen at 50 ^{o}C. It was stirred 12 h. When the reaction was complete 200 ml DI water was added and allowed to stir 2 h at room temperature. Then it was extracted with 1 M HCl (200 ml x 3), 1 M $NaHSO_4$ (200 ml x 3), 10% Na_2CO_3, saturated NaCl (200 ml) and it was dried under anhydrous $MgSO_4$. Ethyl acetate was evaporated to give 5.22 g of colourless oil liquid with a 92% yield. ^{1}H NMR (500 MHz, $CDCl_3$) δ 4.21 (d, J = 11.7 Hz, 4H), 4.13 – 4.09 (m, 4H), 3.68 (d, J = 11.7 Hz, 4H), 3.42 – 3.39 (m, 2H), 1.43 (d, J = 32.2 Hz, 12H), 1.18 (d, J = 1.6 Hz, 6H), 1.08 (d, J = 1.5 Hz, 3H).

A-MPA-4-OH (9)

This procedure was adapted from previously reported procedures.[4] Compound (8) (5.00 g, 10.9 mmol) was dissolved in 20 ml of methanol. 5.00 g of a Dowex, H+ resin was added, and the reaction mixture was stirred for 12 h at 50 ^{o}C. When the reaction was complete the Dowex, H+ resin was filtered off in a vacuum filter under a low vacuum and carefully washed with methanol.

The methanol was evaporated to give 3.96 g of colourless liquid with a 96% yield. ^{1}H NMR (300 MHz, $CDCl_3$) δ 4.09 (s, 4H), 3.88 (d, J = 11.2 Hz, 4H), 3.78 – 3.67 (m, 4H), 3.43 (s, 4H), 3.38 (s, 2H), 1.12 – 1.09 (m, 6H), 1.09 – 1.07 (m, 3H).

A-MPA-4-FA (10)

This procedure was adapted from previously reported procedures.[1] To the stirred solution of (9) (3.25 g, 8.61 mmol), TEA (13.94 g, 138 mmol), 4-dimethylaminopyridine (DMAP) (3.15 g, 25.8 mmol) in 50 ml DCM at 0 ^{o}C under nitrogen, palmitoyl chloride (18.93 g, 68.9 mmol) was dissolved in 20 ml DCM and it was added dropwise. After the complete addition, it was stirred 12 h at room temperature. 150 ml of DI water was added, and it was stirred 1 h. Then the DCM layer was separated, and it was dried under anhydrous $MgSO_4$. DCM was evaporated to give yellow residue further purified by the Sephadex-LH-20 column in DCM to give 10.86 g of yellow solid with a 91% yield. ^{1}H NMR (300 MHz, $CDCl_3$) δ 4.22 (d, J = 1.5 Hz, 8H), 4.01 (s, 4H), 3.32 (s, 2H), 2.30 (t, J = 7.5 Hz, 8H), 1.59 (t, J = 7.4 Hz, 8H), 1.31 (d, J = 5.8 Hz, 104H), 1.04 – 0.99 (m, 3H), 0.91 – 0.86 (m, 18H).

((tetrahydro-2H-pyran-2-yl)oxy)methanamine (11)

This procedure was adapted from previously reported procedures.[5] To the stirred solution of 2-Benzylaminoethanol (5.0 g, 33.1 mmol) in 17 mL of DCM at 0 ^{o}C, methanesulfonic acid (3.50 g, 36.4 mmol) was added at 15 ^{o}C. After 45 min 3,4-dihydro-2H-pyran (4.73 g, 56.2 mmol) was added at 10-15 ^{o}C. It was stirred for 1 h at 15 ^{o}C. Upon ^{1}H NMR confirmation of completion, 3 N caustic solution (17 mL, 49.1 mmol) was added at 5-10 ^{o}C. The phases were separated, and the organic layer was concentrated in the vacuum line. The oily yellow crude product was purified by short path distillation at 3 x 10^3 mbar and 117-125 ^{o}C. 1.0 g of crude product was dissolved in 15 mL of ethanol and Pd/C (5 wt%, 327 mg, 0.154 mmol) was added at room temperature overnight under hydrogen balloon. Upon ^{1}H NMR confirmation of completion, the reaction mixture was filtered through a celite pad. Then the filtrate was concentrated in vacuum to give 0.53 g of compound 11 with 86 % yield. ^{1}H NMR (500 MHz, $CDCl_3$) δ 4.66 – 4.58 (m, 1H), 3.94 – 3.75 (m, 2H), 3.64 (dt, *J* = 16.4, 5.9 Hz, 1H), 3.58 – 3.40 (m, 2H), 2.90 (q, *J* = 11.8, 8.7 Hz, 2H), 1.89 – 1.69 (m, 2H), 1.61 – 1.56 (m, 4H).

P-PAMAM-G-0.5 (12)

To the stirred solution of propargyl amine (5.10 g, 0.0800 mmol) in 50 mL of methanol, methyl acrylate (MA) (35.38 g, 0.410 mmol) in 150 mL of methanol was added dropwise under-salted ice. After the completion of the addition, the reaction mixture was allowed to come to room temperature and then was subjected to heating at 35 ^{o}C overnight. Upon ^{1}H NMR confirmation of completion, MA was co-evaporated in-vacuo three times with butanol, three washes with reagent alcohol, and three with MeOH until complete removal was confirmed by ^{1}H NMR in $CDCl_3$ with

97% yield. ^{1}H NMR (500 MHz, Chloroform-*d*) δ 3.65 (d, *J* = 3.5 Hz, 6H), 2.82 (q, *J* = 7.0, 5.3 Hz, 4H), 2.45 (q, *J* = 7.0, 5.2 Hz, 4H), 2.19 (t, *J* = 2.9 Hz, 1H).

P-PAMAM-G-1.0 (13)

To the stirred solution of ethylenediamine (EDA) (52.1 g, 0.866 mmol) in 100 mL of methanol, 12 (5.09 g, 0.0220 mmol) in 50 mL of methanol was added dropwise under-salted ice. After the completion of the addition, the reaction mixture was allowed to come to room temperature and then was subjected to heating at 35 ^{o}C overnight. Upon ^{1}H NMR confirmation of completion, MA was co-evaporated in-vacuo three times each with butanol, reagent alcohol, and MeOH until complete removal was confirmed by ^{1}H NMR in MeOD with 90% yield. ^{1}H NMR (500 MHz, MeOD) δ 3.58 (t, J = 6.5 Hz, 5H), 3.53 – 3.47 (m, 2H), 3.28 (t, J = 6.2 Hz, 4H), 2.86 (t, J = 6.7 Hz, 5H), 2.75 (t, J = 6.2 Hz, 5H), 2.65 (t, J = 2.6 Hz, 1H), 2.41 (t, J = 6.7 Hz, 4H), 2.20 (t, *J* = 2.9 Hz, 1H).

P-PAMAM-G-1.5 (14)

To the stirred solution of MA (53.30 g, 0.620 mmol) in 200 mL of methanol, 13 (5.94 g, 0.0620 mmol) in 50 mL in methanol was added dropwise under-salted ice. After the completion of the addition, the reaction mixture was allowed to come to room temperature and then was subjected to heating at 35 ^{o}C for two days. Upon ^{1}H NMR confirmation of completion, MA was co-evaporated in-vacuo three times with butanol, three with reagent alcohol, and three with MeOH until complete removal was confirmed by ^{1}H NMR in $CDCl_3$ with 95% yield. ^{1}H NMR (500 MHz, $CDCl_3$) δ 3.70 (d, J = 1.5 Hz, 13H), 3.49 (d, J = 2.2 Hz, 2H), 3.32 (q, J = 5.8 Hz, 4H), 2.88 (t, J = 6.7 Hz, 4H), 2.79 (t, J = 6.6 Hz, 9H), 2.57 (t, J = 6.0 Hz, 3H), 2.46 (t, J = 6.7 Hz, 9H), 2.41 (t, J = 6.8 Hz, 4H), 2.19 (t, *J* = 2.9 Hz, 1H).

P-PAMAM-G-2.0 (15)

To the stirred solution of EDA (47.56 g, 793 mmol) in 100 mL of methanol, 14 (12.51g, 9.87 mmol) in 60 mL in methanol was added dropwise under-salted ice. After the completion of the addition, the reaction mixture was allowed to come to room temperature and then it was subjected to heating at 35 ^{o}C for three days. Upon ^{1}H NMR confirmation of completion, MA was co-evaporated in-vacuo three times with butanol, three with reagent alcohol, and three with MeOH until complete removal was confirmed by ^{1}H NMR in MeOD with 91% yield. ^{1}H NMR (500 MHz, $CDCl_3$) δ 3.56 (t, J = 6.7 Hz, 12H), 3.39 (t, J = 4.7 Hz, 2H), 3.21 (m, J = 12.0, 6.0 Hz, 8H), 2.76 (t, J = 5.9 Hz, 8H), 2.69 (dd, J = 11.0, 4.7 Hz, 8H), 2.47 (t, J = 6.2 Hz, 2H), 2.29 (d, J = 21.8 Hz, 18H), 2.20 (t, *J* = 2.9 Hz, 1H).

P-PAMAM-G-2.5 (16)

To the stirred solution of MA (71.84 g, 834 mmol) in 150 mL of methanol, 15 (12.45 g, 16.7 mmol) in 60 mL in methanol was added dropwise under-salted ice. After the completion of the

addition, the reaction mixture was allowed to come to room temperature and then it was subjected to heating at 35 ^{o}C for four days. Upon ^{1}H NMR confirmation of completion, MA was co-evaporated in-vacuo three times with butanol, three with reagent alcohol, and three with MeOH until complete removal was confirmed by ^{1}H NMR in $CDCl_3$ with 94% yield. ^{1}H NMR (300 MHz, $CDCl_3$) δ 3.68 (s, 24H), 3.47 (s, 2H), 3.30 (d, J = 5.8 Hz, 12H), 2.79 (dt, J = 13.6, 6.5 Hz, 28H), 2.57 (dt, J = 12.2, 6.0 Hz, 12H), 2.44 (t, J = 6.7 Hz, 16H), 2.38 (t, J = 6.3 Hz, 12H), 2.19 (t, *J* = 2.9 Hz, 1H).

P-PAMAM-G-3.0 (17)

To the stirred solution of EDA (34.31 g, 571 mmol) in 70 mL of methanol, 16 (10.24 g, 7.14 mmol) in 50 mL in methanol was added dropwise under-salted ice. After the completion of the addition, the reaction mixture was allowed to come to room temperature and then it was subjected to heating at 35 ^{o}C for four days. Upon ^{1}H NMR confirmation of completion, MA was co-evaporated in-vacuo three times with butanol, three with reagent alcohol, and three with MeOH until complete removal was confirmed by ^{1}H NMR in MeOD with an 88% yield. ^{1}H NMR (500 MHz, MeOD) δ 3.57 (t, J = 6.7 Hz, 4H), 3.39 – 3.34 (m, 16H), 3.32 – 3.26 (m, 28H), 2.81 (tq, J = 12.8, 6.4 Hz, 48H), 2.61 (q, J = 6.8 Hz, 14H), 2.39 (t, J = 7.0 Hz, 30H).

P-PAMAM-TBE (18)

To the stirred solution of 15 (22.00 g, 29.7 mmol) in 110 mL of methanol, tertbutyl acrylate (TBA) (190.53 g, 149 mmol) in 380 mL methanol was added dropwise under-salted ice. After the complete addition of TBA, the reaction was allowed to warm to room temperature. The reaction continued at room temperature for two days. Upon ^{1}H NMR confirmation of completion, a single rotovap ensued. The PAMAM product was dissolved into a minimal amount of DCM which was followed by precipitation via separatory funnel into 5x mL of stirring, pure hexane. After settling, the hexane layer was decanted, and the remaining product was air-dried. This precipitation, decanting, and the air-drying process was repeated twice more. A final ^{1}H NMR ensured the removal of TBA with 90% yield. ^{1}H NMR (500 MHz, $CDCl_3$) δ 3.47 (s, 2H), 3.35 (s, 18H), 3.26 (s, 26H), 2.74 (s, 24H), 2.56 (d, J = 15.4 Hz, 14H), 2.37 (s, 28H), 2.19 (t, *J* = 2.9 Hz, 1H), 1.45 (s, 72H).

P-PAMAM-BOC (19)

To the stirred solution of 17 (15.06 g, 9.04 mmol) in 150 mL of methanol, di-tert-butyl dicarbonate (Boc Anhydride) (39.85 g, 0.182 mmol) in 120 mL in methanol was added dropwise under-salted ice. After the complete addition of Boc Anhydride, the reaction was allowed to warm to room temperature. The reaction continued at room temperature for two days. Upon ^{1}H NMR confirmation of completion, a single rotovap ensued. The PAMAM product was dissolved into a minimal amount of DCM which was followed by precipitation via separatory funnel into 5x mL of stirring, pure hexane. After settling, the hexane layer was decanted, and the remaining product

was air-dried. This precipitation, decanting, and the air-drying process was repeated twice more. A final ^{1}H NMR ensured the removal of Boc Anhydride with a 92% yield. ^{1}H NMR (400 MHz, $CDCl_3$) δ 3.62 (s, 2H), 3.32 (q, J = 5.6 Hz, 18H), 3.24 (t, J = 6.2 Hz, 28H), 2.80 – 2.65 (m, 28H), 2.53 (q, J = 7.9, 6.0 Hz, 14H), 2.36 (q, J = 9.0, 6.7 Hz, 28H), 2.23 (s, 1H), 1.42 (s, 72H).

P-PAMAM-THP (20)

To the stirred solution of 16 (15.06 g, 9.04 mmol) in 150 mL of methanol, ((tetrahydro-2H-pyran-2-yl)oxy)methanamine (THP) (11) (39.85 g, 0.182 mmol) in 120 mL in methanol was added dropwise under-salted ice. After the complete addition of THP, the reaction was allowed to warm to room temperature. The reaction continued at room temperature for four days. Upon ^{1}H NMR confirmation of completion, a single rotovap ensued. The PAMAM product was dissolved into a minimal amount of DCM which was followed by precipitation via separatory funnel into 5x mL of stirring, pure hexane. After settling, the hexane layer was decanted, and the remaining product was air-dried. This precipitation, decanting, and the air-drying process was repeated twice more. It was further purified using size exclusion chromatography (Sephadex LH-20). A final ^{1}H NMR ensured the removal of excess THP with 81% yield. ^{1}H NMR (500 MHz, $CDCl_3$) δ 4.57 (s, 8H), 3.94 – 3.72 (m, 18H), 3.48 (d, J = 31.1 Hz, 28H), 3.34 (s, 12H), 2.97 – 2.61 (m, 24H), 2.36 (s, 16H), 1.81 (s, 52H), 1.63 – 1.36 (m, 48H).

Reported below are the full synthetic details for the preparation of macromolecules

FA-PAMAM-NH_3^+

To the stirred solution of P-PAMAM-Boc (3.20 g, 1.31 mmol), A-MPA-4-FA (2.72 g, 1.957 mmol) in 25 ml of DMF, CuBr (374.0 mg, 2.61 mmol) was added under nitrogen flushing. After complete addition, N,N,N′,N″,N″-Pentamethyldiethylenetriamine (PMDETA) (452.2 mg, 2.61 mmol) was added and allowed to stir under nitrogen at 35 ^{o}C for 48 h. The reaction mixture was precipitated to 200 ml diethyl ether. After settling, the diethyl ether layer was decanted, and the remaining product was air-dried. This precipitation, decanting, and the air-drying process was repeated twice more. The crude product was dissolved in 100 ml of DCM. It was extracted with 0.1 M EDTA solution. It was further purified using size exclusion chromatography (Sephadex LH-20) to give 3.95 g of FA-PAMAM-BOC. It was dissolved in 45 ml of chloroform and 4.5 mL (10% v/v) of trifluoroacetic acid (TFA) was slowly added and stirred for 45 minutes. The reaction mixture was air-dried and dissolved in 10 mL of chloroform. It was added dropwise to 500 mL of diethyl ether and stirred for 2 h. It was filtered and precipitation procedure was repeated three times. Finally, the resulting yellow solid was put under the vacuum for 24 hours to obtain the pure product with 86% yield. ^{1}H NMR for FA-PAMAM-Boc (500 MHz, $CDCl_3$) δ 7.87 (s, 1H), 5.87-5.70 (m, 8H), 4.40 (s, 2H), 4.29 (s, 2H), 4.26 (s, 4H), 4.23 (s, 8H), 3.31 (m, 28H), 3.23 (m, 18H), 2.81 (m, 28H), 2.49 (m, 14H), 2.29 (q, 28H) ,1.42 (s, 72H), 1.30-1.22 (m, 104H), 1.01 (s, 3H),

0.98 (s, 6H), 0.86 (t, 12H). ^{13}C NMR (101 MHz, Chloroform-*d*) δ 172.99, 172.07, 156.40, 144.29, 125.79, 78.99, 77.40, 64.87, 52.45, 47.84, 44.21, 33.97, 31.81, 29.58, 24.80, 22.56, 17.73, 13.95.

FA-PAMAM-COOH

To the stirred solution of P-PAMAM-TBE (2.50 g, 1.32 mmol), A-MPA-4-FA (1.67 g, 1.29 mmol) in 25 ml of DMF, CuBr (374.0 mg, 2.61 mmol) was added under nitrogen flushing. After complete addition, PMDETA (452.2 mg, 2.61 mmol) was added and allowed to stir under nitrogen at 35 ^{o}C for 48 h. The reaction mixture was precipitated to 200 ml diethyl ether. After settling, the diethyl ether layer was decanted, and the remaining product was air-dried. This precipitation, decanting, and the air-drying process was repeated twice more. The crude product was dissolved in 100 ml of DCM. It was extracted with 0.1 M EDTA solution. It was further purified using size exclusion chromatography (Sephadex LH-20) to give FA-PAMAM-TBE as a yellow solid. Then 2 g of FA-PAMAM-TBE was dissolved in 30 ml of chloroform and 3.0 mL (10% v/v) of TFA was added dropwise and stirred for 45 minutes. The reaction mixture was air-dried and dissolved in 8 mL of chloroform. It was added dropwise to 500 mL of diethyl ether and stirred for 2 h. It was filtered and precipitation procedure was repeated three times. Finally, the resulting yellow solid was put under the vacuum for 24 h to obtain the pure product with 82% yield. ^{1}H NMR for FA-PAMAM-TBE (400 MHz, $CDCl_3$) δ 7.82 (s, 1H), 5.91-5.60 (m, 4H), 4.39 (s, 2H), 4.29 (s, 2H), 4.26 (s, 4H), 4.22 (s, 8H), 4.01 (s, 8H), 3.32 (m, 18H), 3.22 (m, 26H), 2.84 (s, 24H), 2.47 (s, 28H), 2.30 (t, 14H), 1.42 (s, 72H), 1.27 – 1.24 (m, 104H), 1.01 (s, 3H), 0.98 (s, 6H), 0.89 – 0.87 (m, 14H).^{13}C NMR (126 MHz, $CDCl_3$) δ 173.13, 171.92, 162.49, 142.91, 125.24, 66.00, 64.86, 52.81, 52.49, 51.60, 49.19, 46.47, 37.16, 36.42, 34.60, 29.65, 25.21, 24.81, 17.82, 14.05.

FA-PAMAM-OH

To the stirred solution of P-PAMAM-THP (1.04 g, 0.428 mmol), A-MPA-4-FA (0.86 g, 0.642 mmol) in 10 ml of DMF, CuBr (130.0 mg, 0.856 mmol) was added under nitrogen flushing. After complete addition, PMDETA (149.4 mg, 0.856 mmol) was added and allowed to stir under nitrogen at 35 ^{o}C for 48 h. The reaction mixture was precipitated to 200 ml diethyl ether. After settling, the diethyl ether layer was decanted, and the remaining product was air-dried. This precipitation, decanting, and the air-drying process was repeated twice more. The crude product was dissolved in 100 ml of DCM. It was extracted with 0.1 M EDTA solution. It was further purified using size exclusion chromatography (Sephadex LH-20) to give 1.27 g of a solid. Then 1g of FA-PAMAM-THP was dissolved in 15 ml of chloroform and 2.0 mL of TFA was added dropwise and stirred for 60 minutes. The reaction mixture was air-dried and dissolved in 5 mL of chloroform. It was added dropwise to 250 mL of diethyl ether:methanol mixture (2:1) and stirred for 2 h. It was filtered and precipitation procedure was repeated three times. Finally, the resulting yellow solid was put under the vacuum for 24 h to obtain the pure product with a 79 % yield. ^{1}H

NMR for FA-PAMAM-THP (400 MHz, $CDCl_3$) δ 7.89 (s, 1H), 4.60 (s, 8H), 4.25 (s, 8H), 3.89 (s, 28H), 3.55 (s, 18H), 2.32 (s, 12H), 1.36 – 1.23 (m, 104H), 0.91 (s, 18H). ^{13}C NMR (101 MHz, Chloroform-*d*) δ 174.10, 172.96, 162.45, 142.04, 125.99, 98.88, 77.32, 66.30, 65.08, 63.76, 54.91, 46.50, 39.57, 34.05, 31.95, , 29.72, 25.47, 22.73, 22.71, 19.69, 17.87, 13.96.

NMR SPECTRA

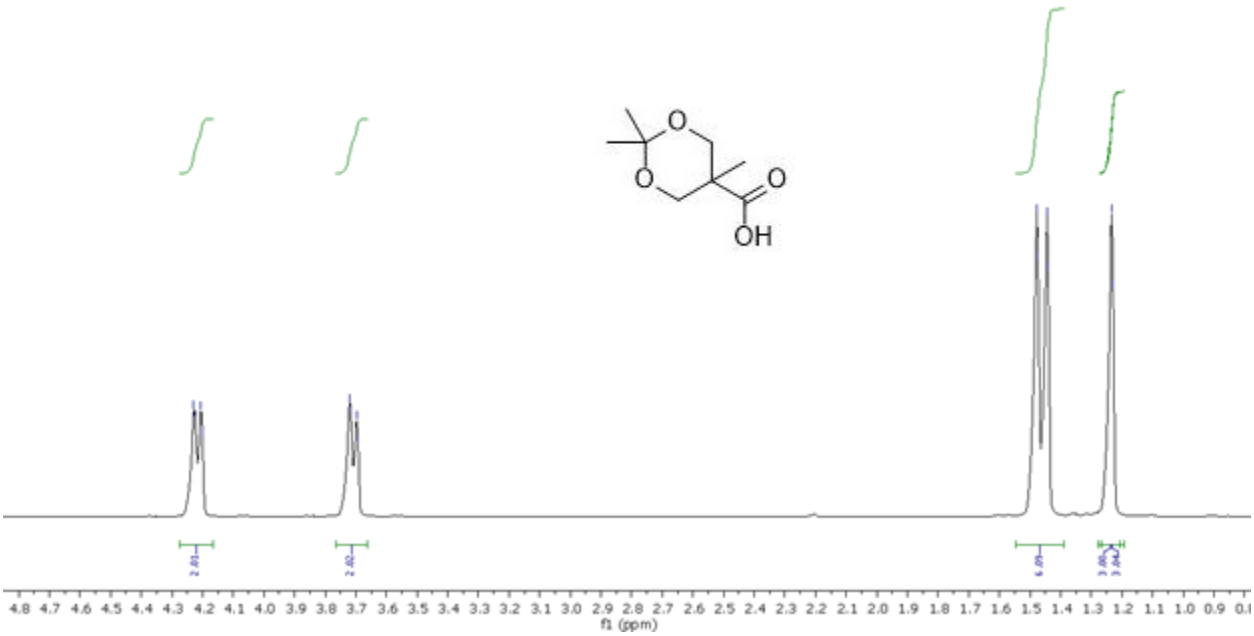

Figure S1. ^{1}H NMR for 2,2,5-trimethyl-1,3-dioxane-5-carboxylic acid (2**)** (500 MHz, $CDCl_3$)

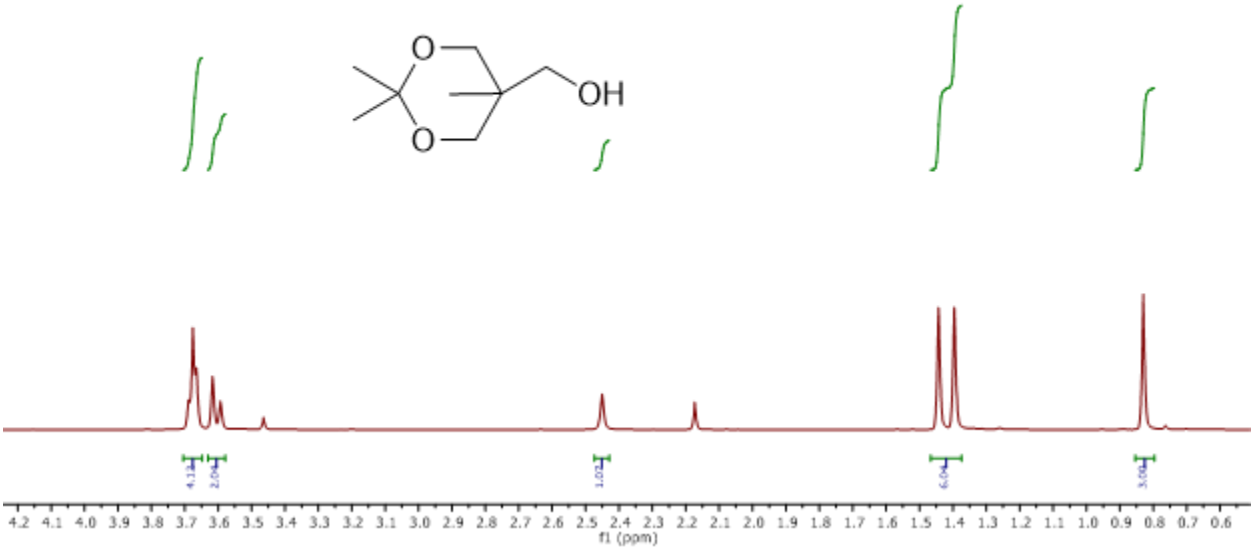

Figure S2. ^{1}H NMR for (2,2,5-trimethyl-1,3-dioxan-5-yl)methanol (4) (500 MHz, $CDCl_3$)

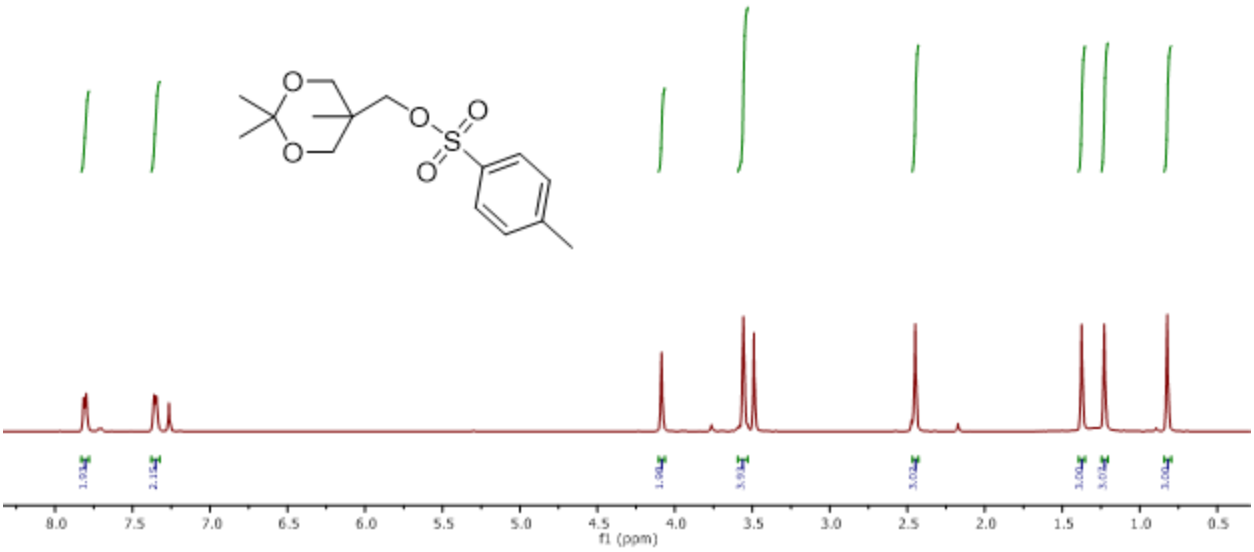

Figure S3. ^{1}H NMR for (2,2,5-trimethyl-1,3-dioxan-5-yl)methyl 4-methylbenzenesulfonate (5) (500 MHz, $CDCl_3$)

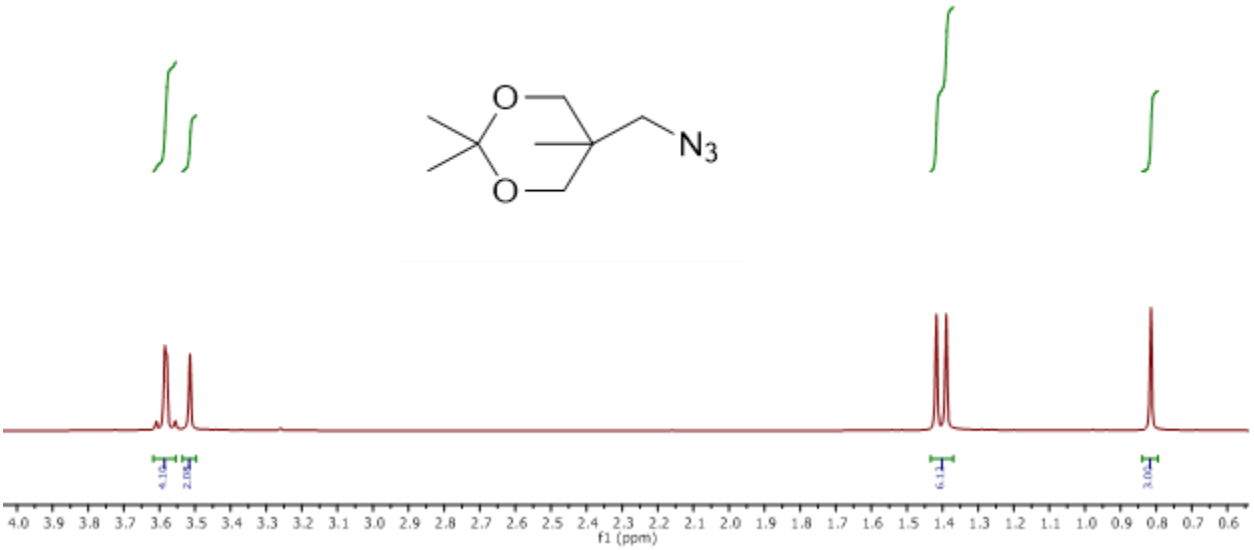

Figure S4. ^{1}H NMR for 5-(azidomethyl)-2,2,5-trimethyl-1,3-dioxane (6) (500 MHz, $CDCl_3$)

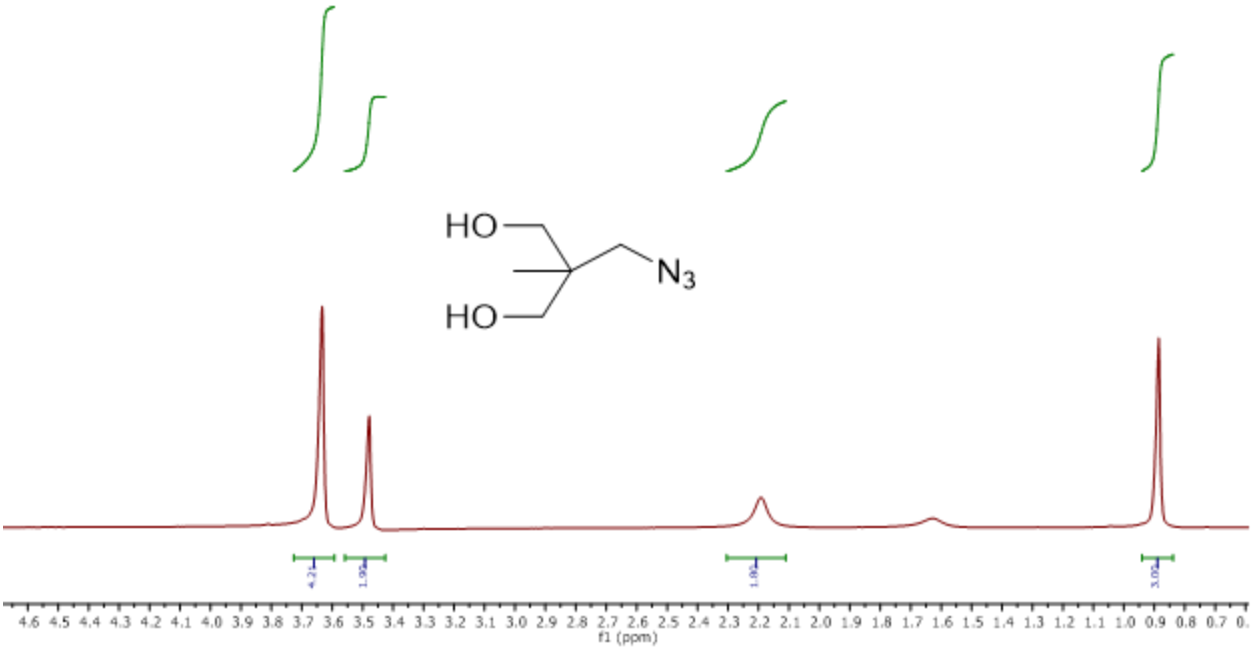

Figure S5. ^{1}H NMR for 2-(azidomethyl)-2-methylpropane-1,3-diol (7) (400 MHz, $CDCl_3$)

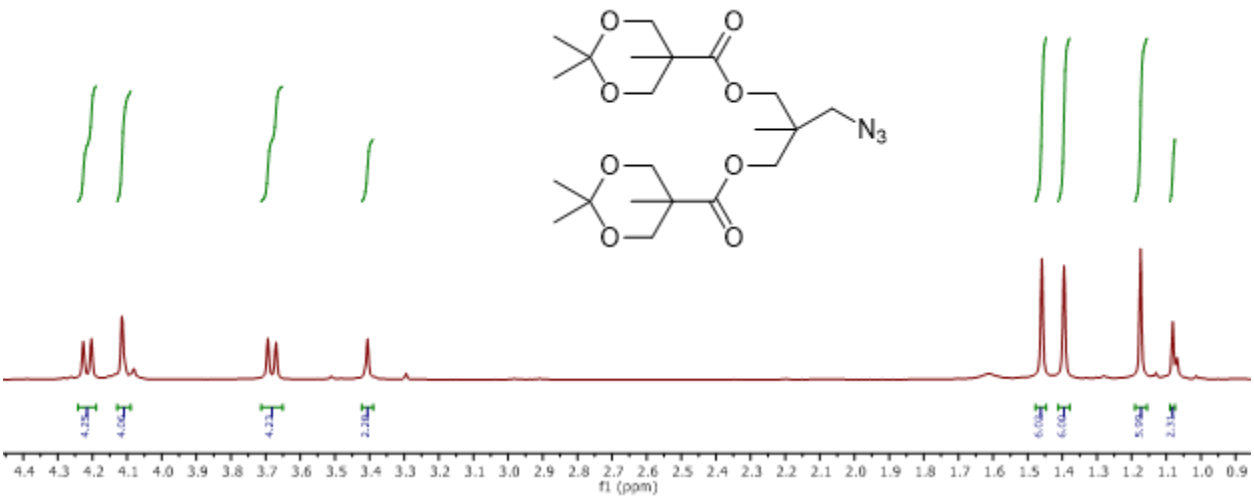

Figure S6. ^{1}H NMR for A-MPA-4-AC (8) (400 MHz, $CDCl_3$)

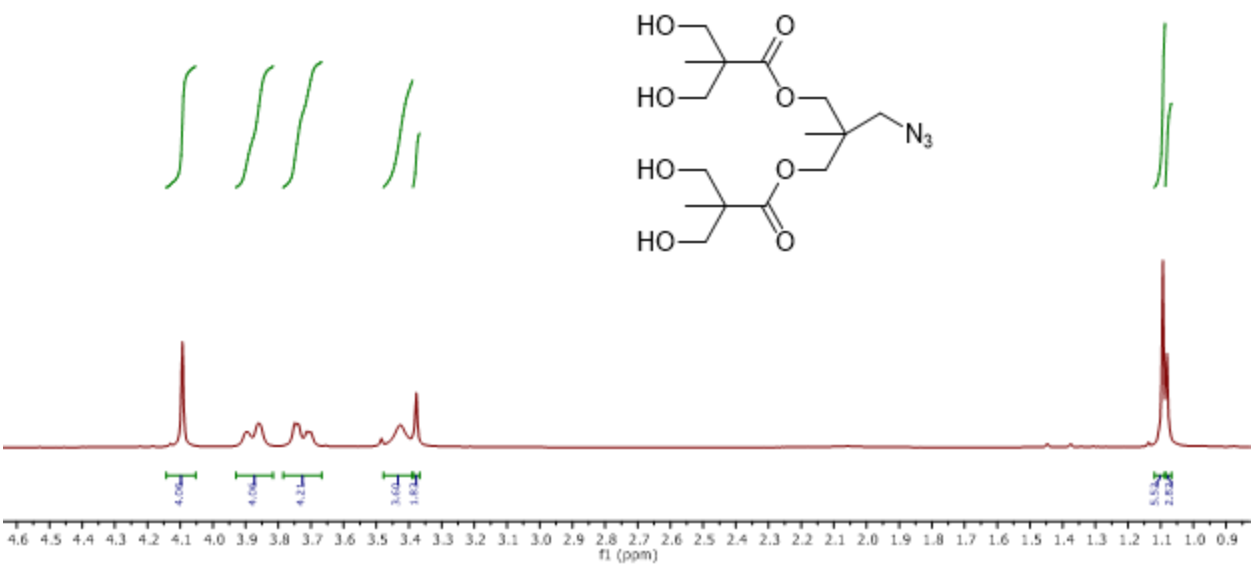

Figure S7. ^{1}H NMR for A-MPA-4-OH (9) (400 MHz, $CDCl_3$)

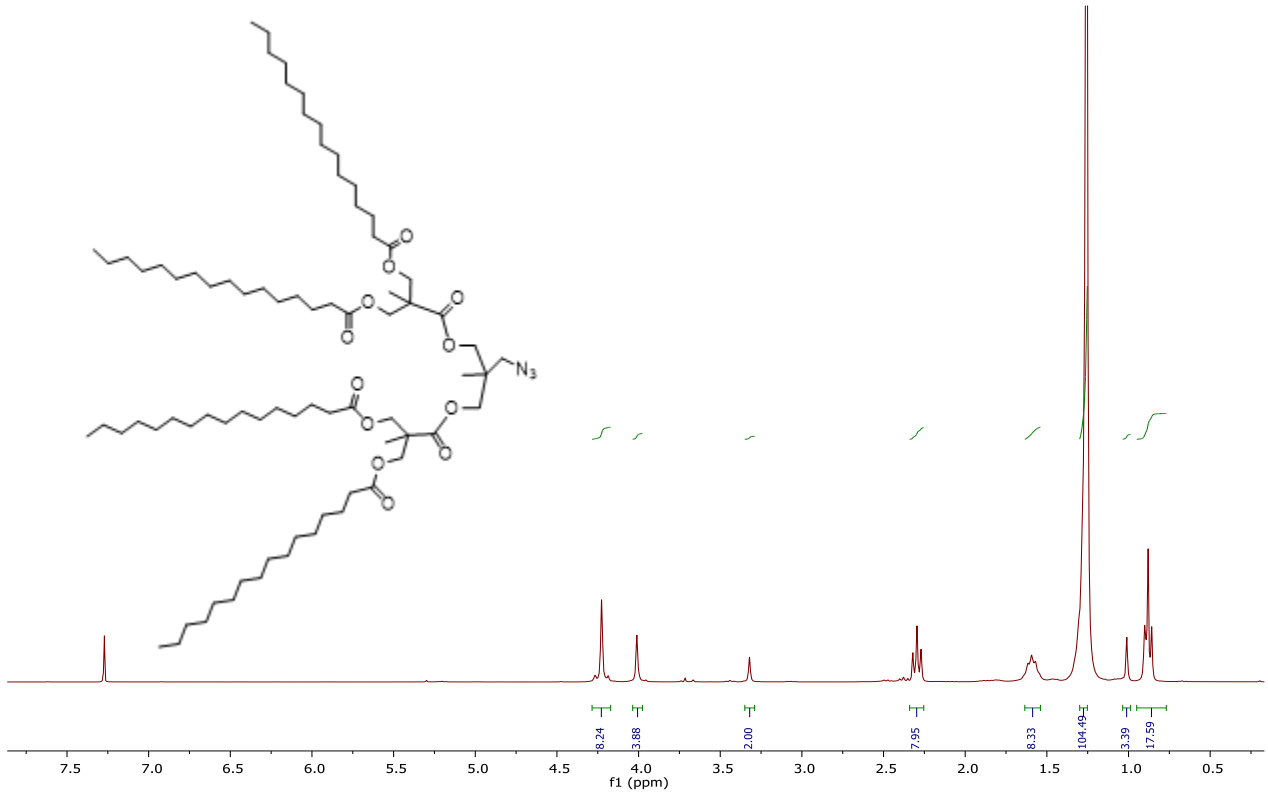

Figure S8. ^{1}H NMR for A-MPA-4-FA (10) (400 MHz, $CDCl_3$)

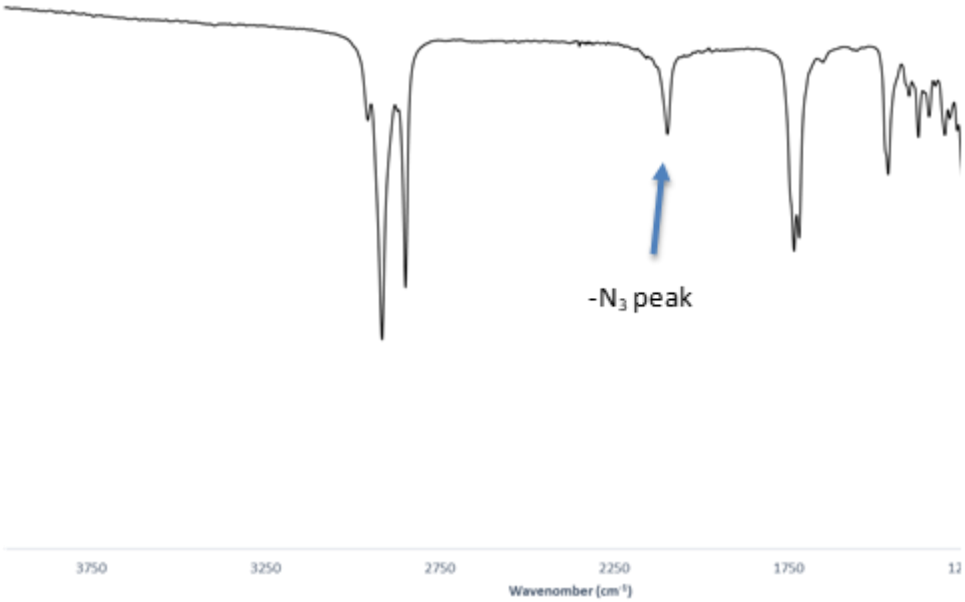

Figure S9. FTIR spectra for A-MPA-4-FA (10)

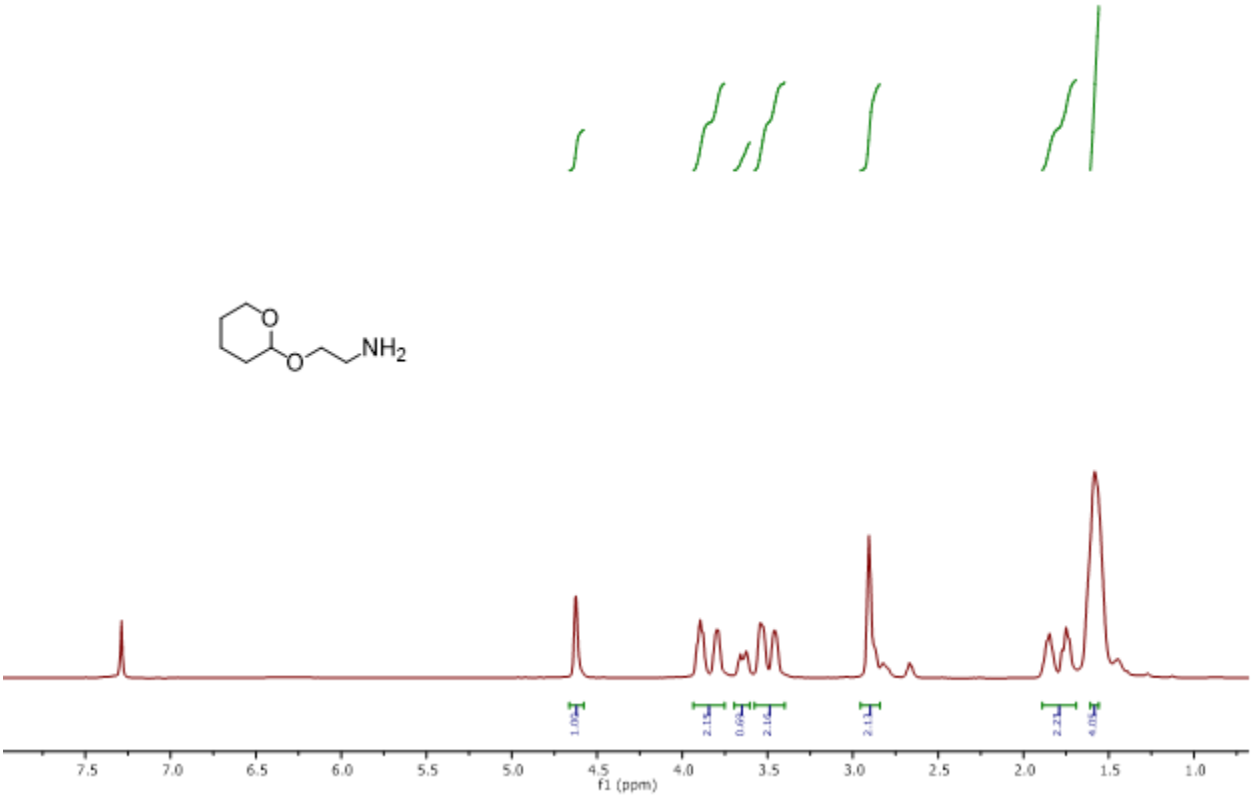

Figure S10. ^{1}H NMR for ((tetrahydro-2H-pyran-2-yl)oxy)methanamine (11) (500 MHz, $CDCl_3$)

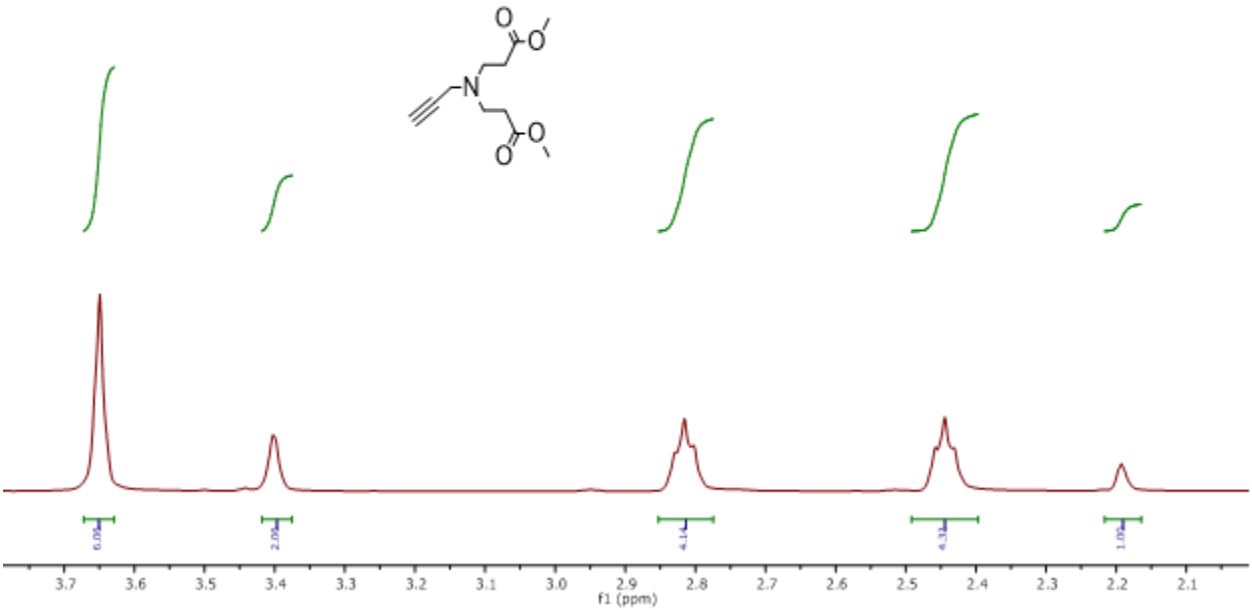

Figure S11. ^{1}H NMR for P-PAMAM-G0.5 (500 MHz, $CDCl_3$)

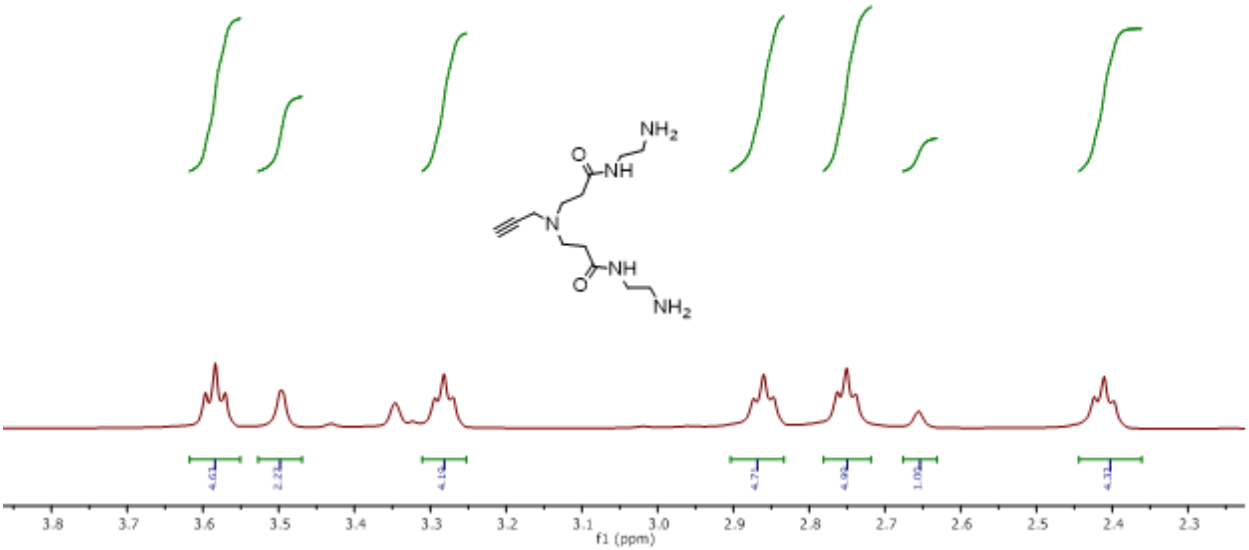

Figure S12. ^{1}H NMR for P-PAMAM-G1.0 (500 MHz, MeOD)

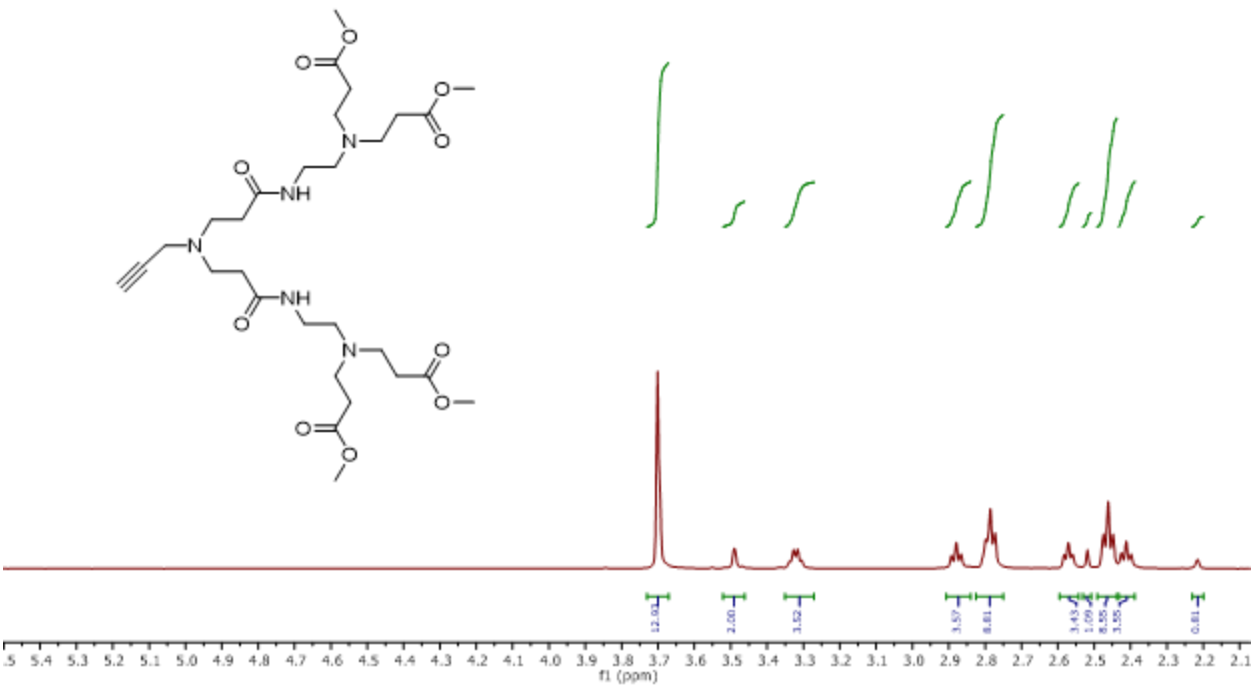

Figure S13. ^{1}H NMR for P-PAMAM-G1.5 (500 MHz, $CDCl_3$)

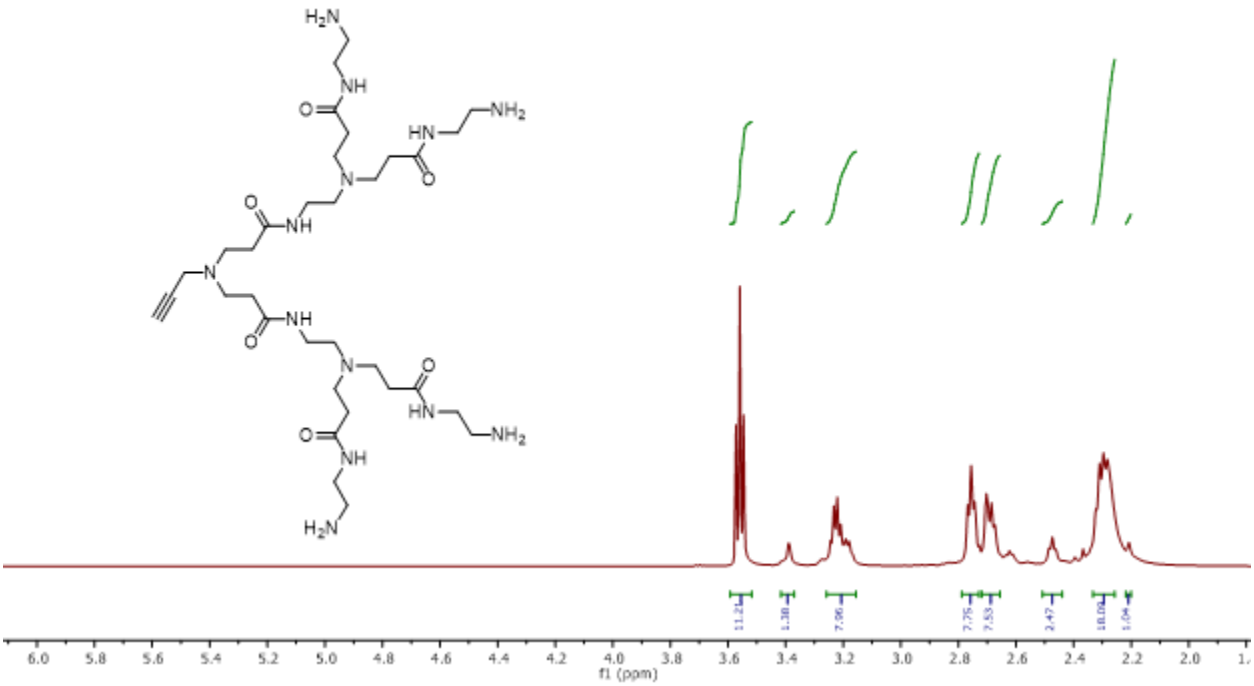

Figure S14. ^{1}H NMR for P-PAMAM-G2.0 (500 MHz, MeOD)

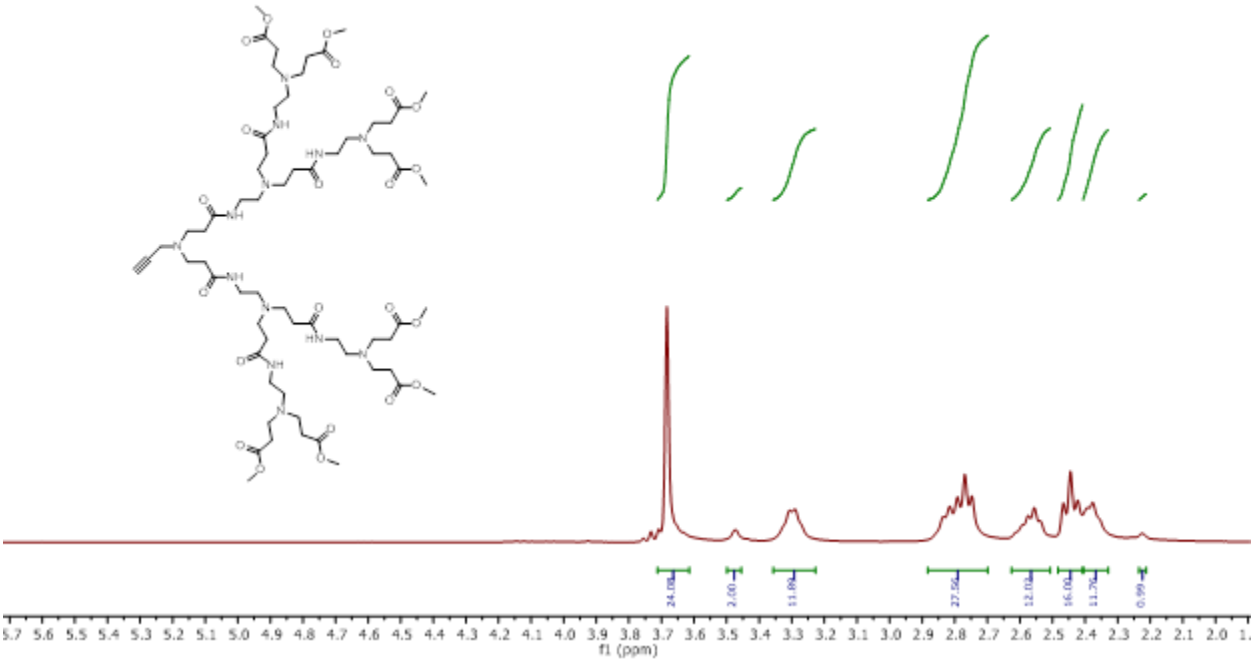

Figure S15. ^{1}H NMR for P-PAMAM-G2.5 (500 MHz, $CDCl_3$)

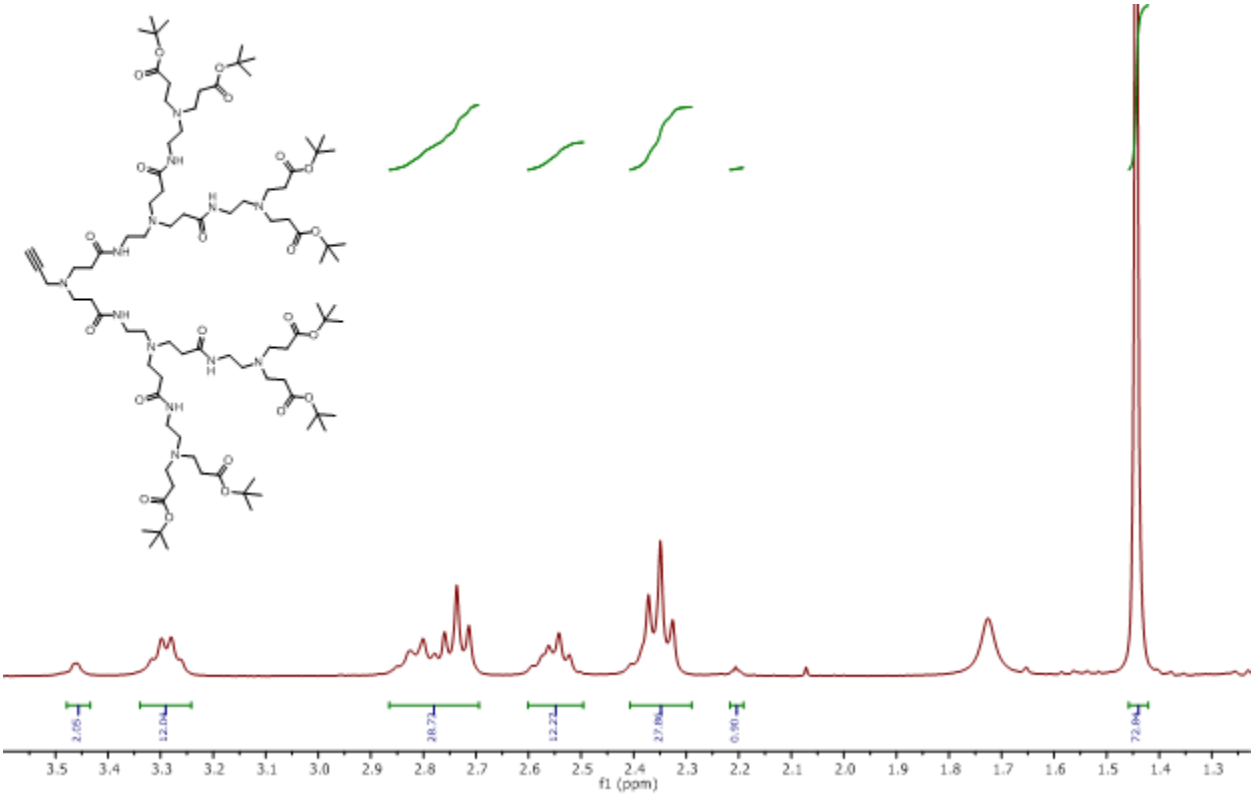

Figure S16. ^{1}H NMR for P-PAMAM-TBE (300 MHz, $CDCl_3$)

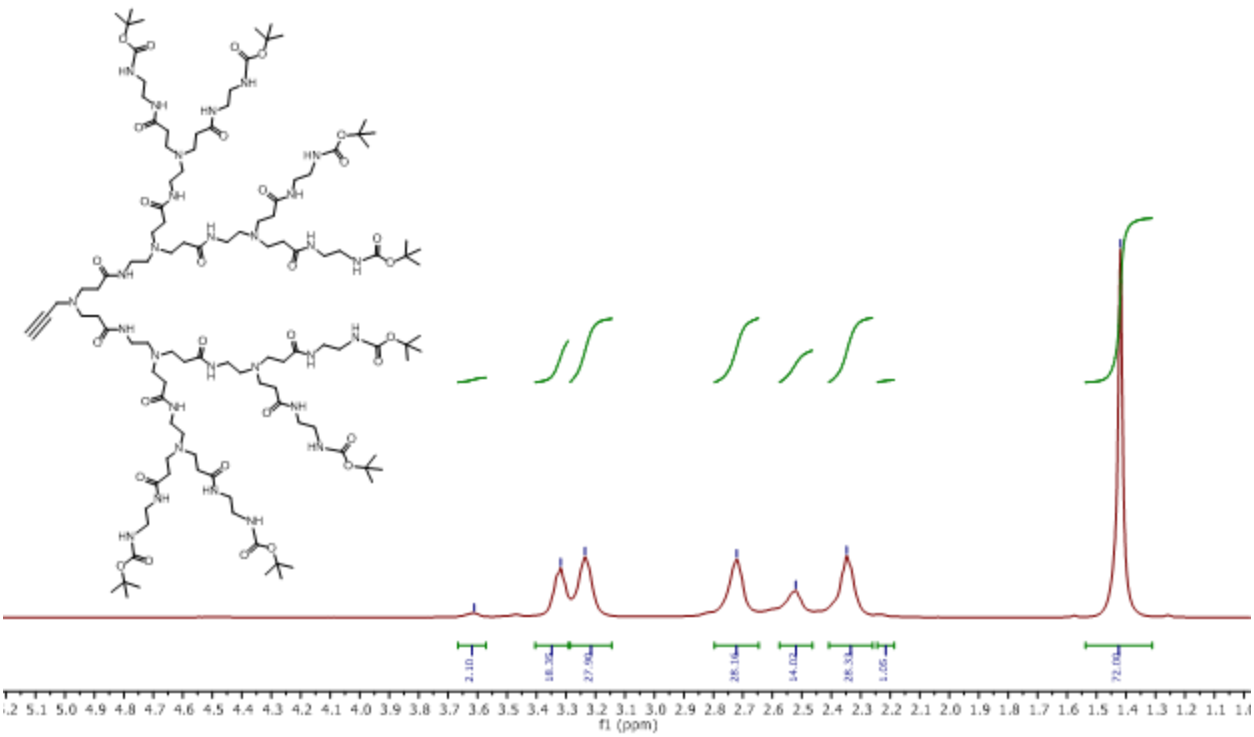

Figure S17. ^{1}H NMR for P-PAMAM-BOC (400 MHz, $CDCl_3$)

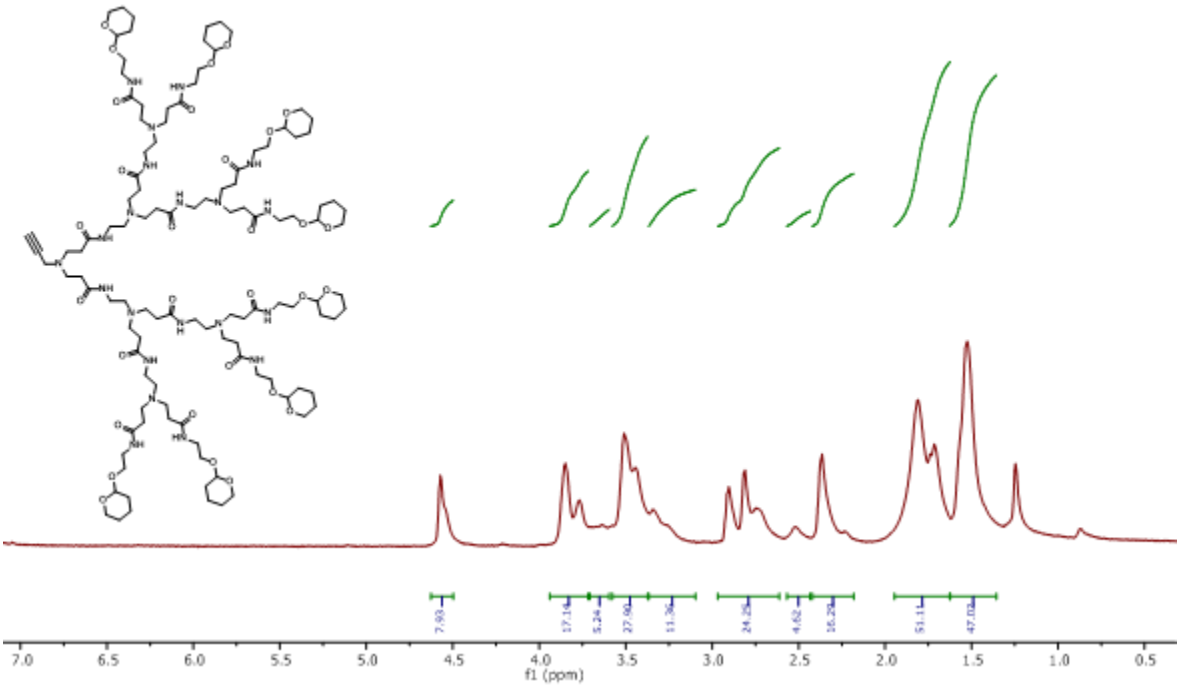

Figure S18. ^{1}H NMR for P-PAMAM-G-3.0-THP (500 MHz, $CDCl_3$)

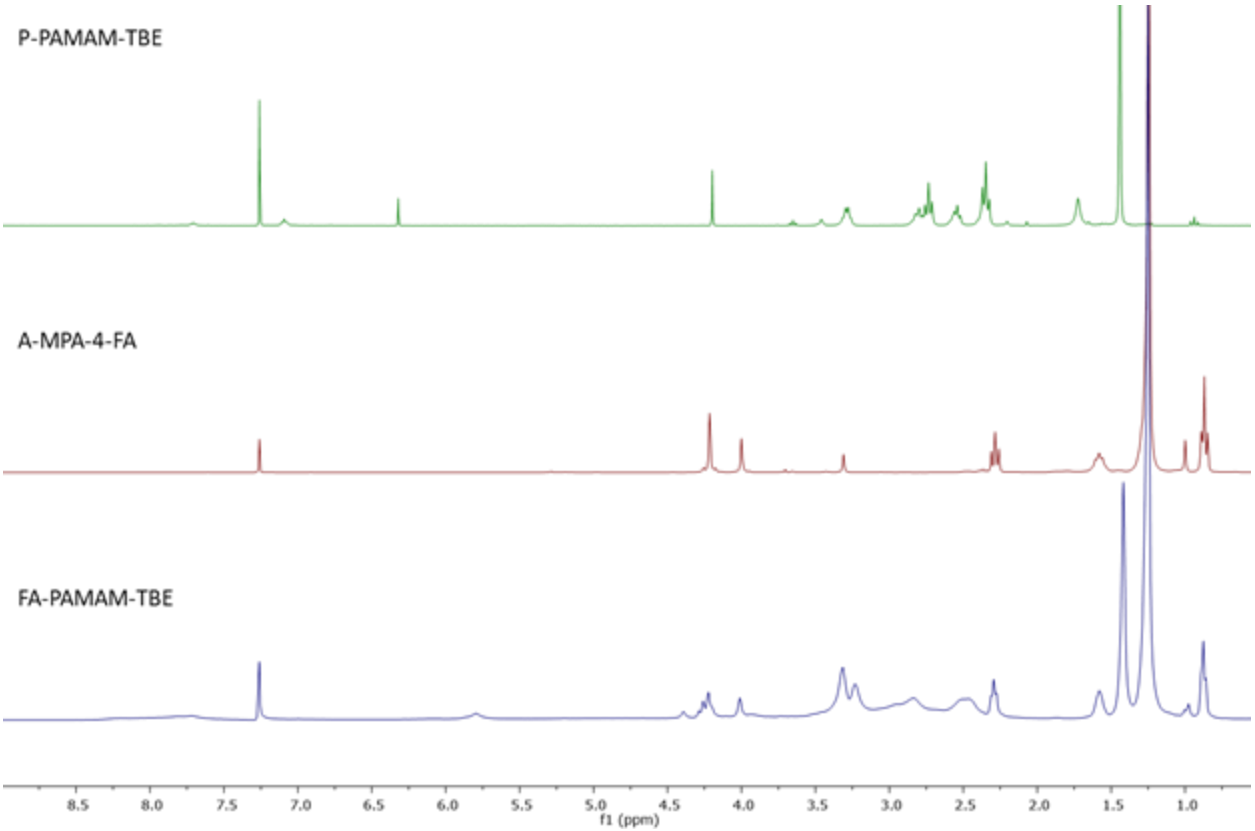

Figure S19. ^{1}H NMR comparison for FA-PAMAM-TBE with P-PAMAM-TBE and A-MPA-4-FA (500 MHz, $CDCl_3$)

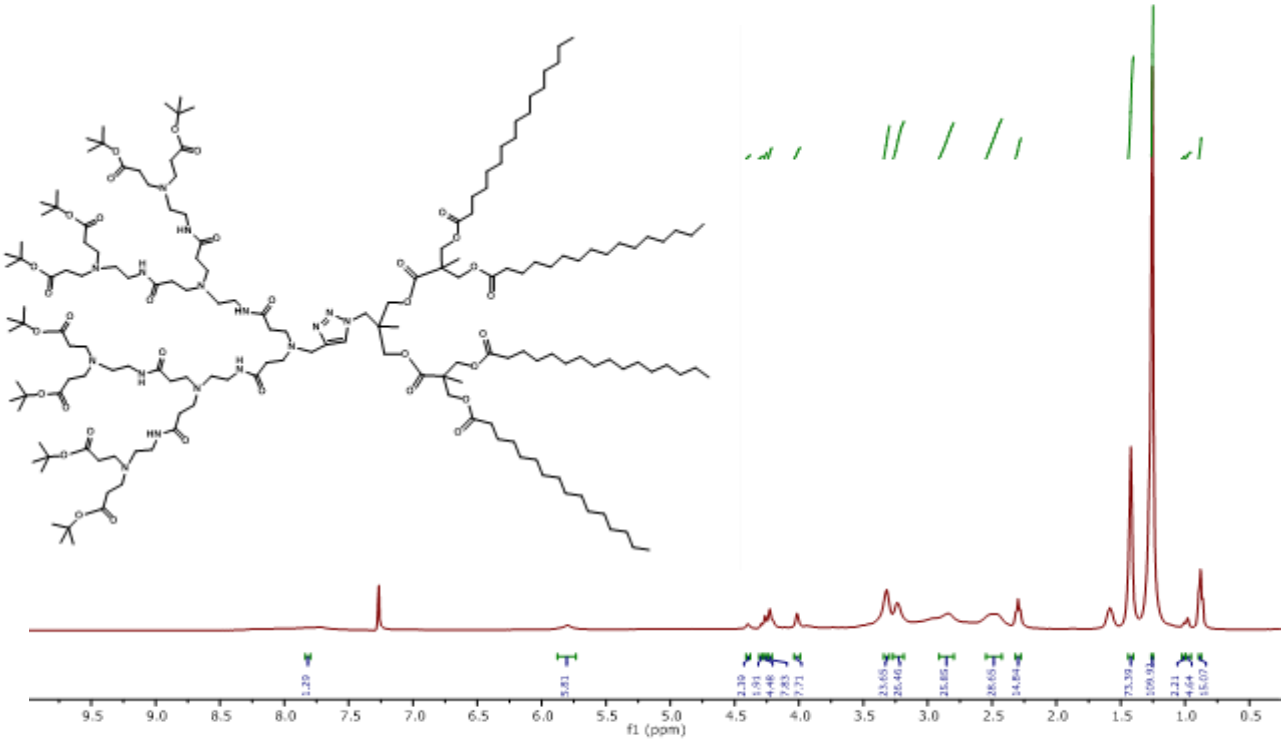

Figure S20. ^{1}H NMR for FA-PAMAM-TBE (500 MHz, $CDCl_3$)

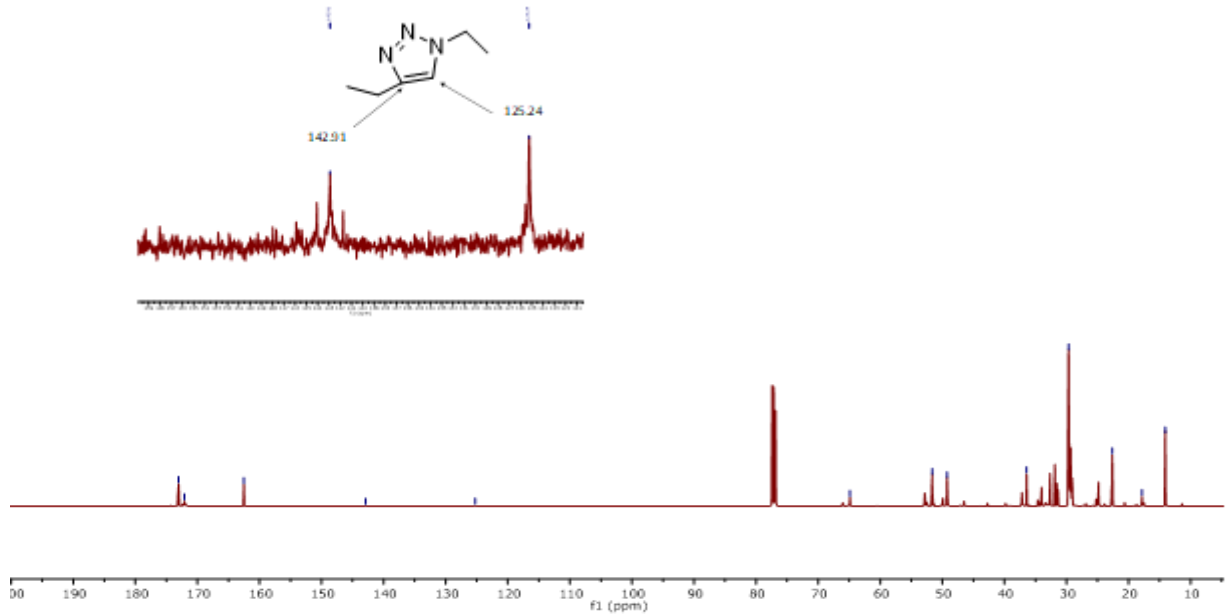

Figure S21. ^{13}C NMR for FA-PAMAM-TBE (300 MHz, $CDCl_3$)

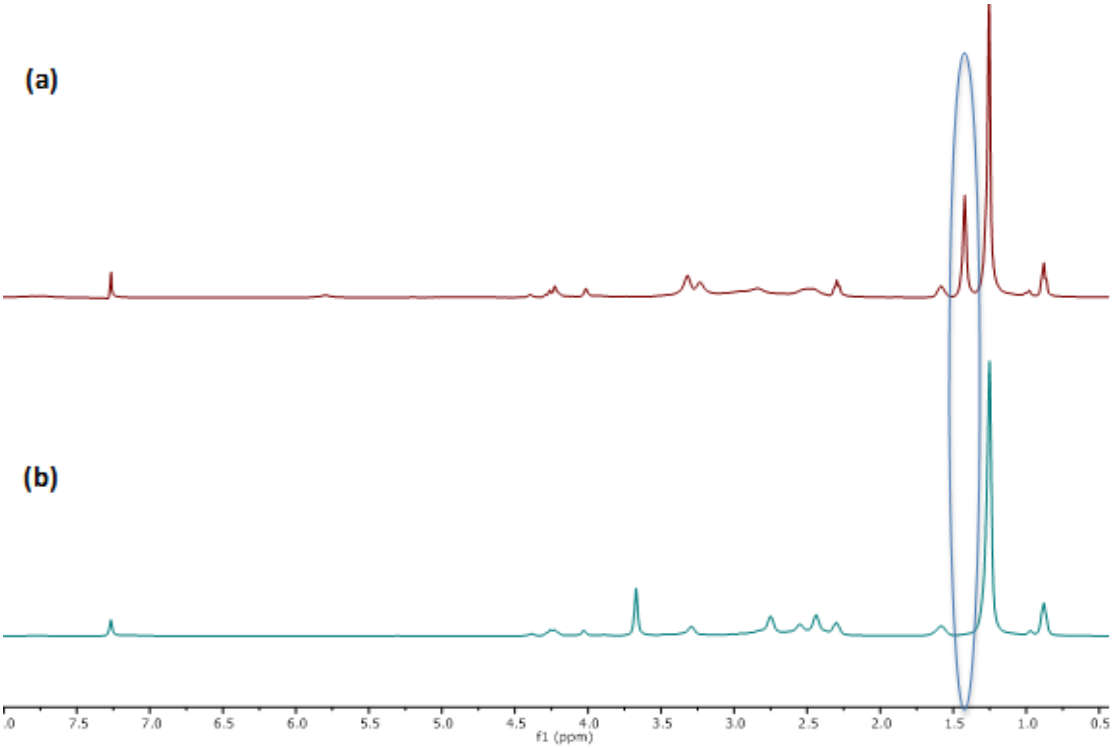

Figure S22. ^{1}H NMR comparison for (a) FA-PAMAM-TBE, (b) FA-PAMAM-COOH (500 MHz, $CDCl_3$)

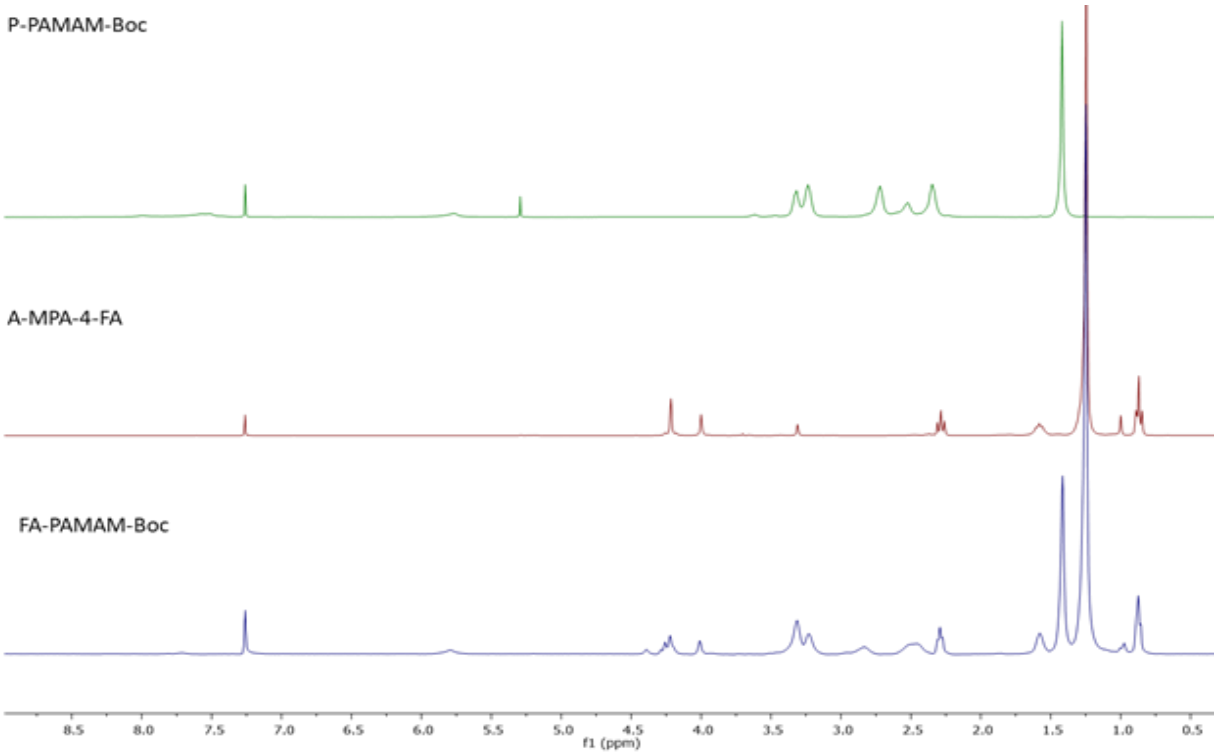

Figure S23. ^{1}H NMR comparison for FA-PAMAM-BOC with P-PAMAM-BOC and A-MPA-4-FA (500 MHz, $CDCl_3$)

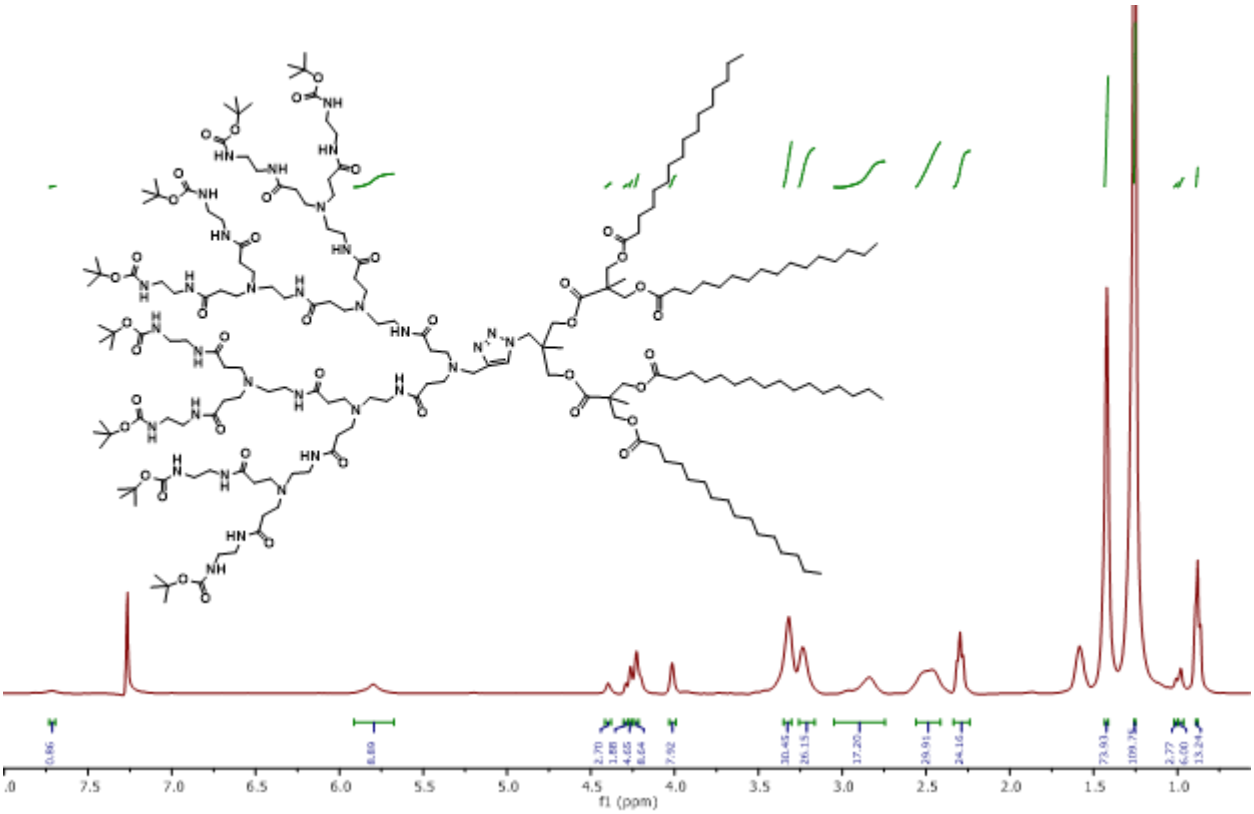

Figure S24. ^{1}H NMR for FA-PAMAM-BOC (500 MHz, $CDCl_3$)

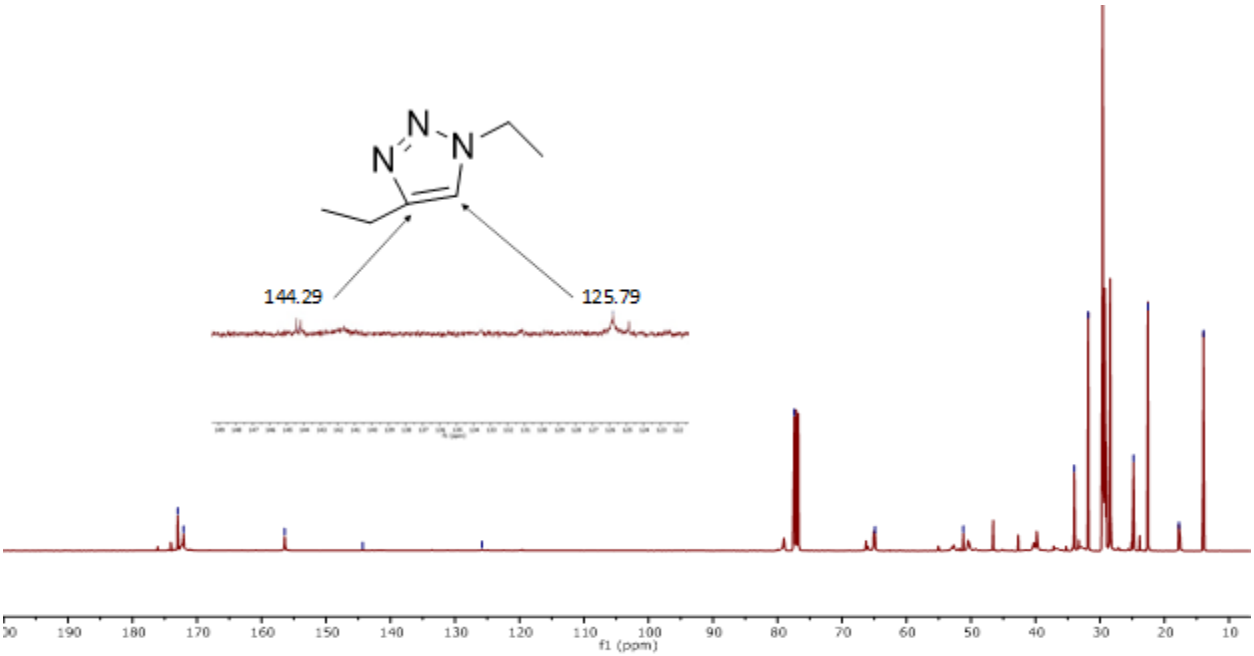

Figure S25. ^{13}C NMR for FA-PAMAM-BOC (400 MHz, $CDCl_3$)

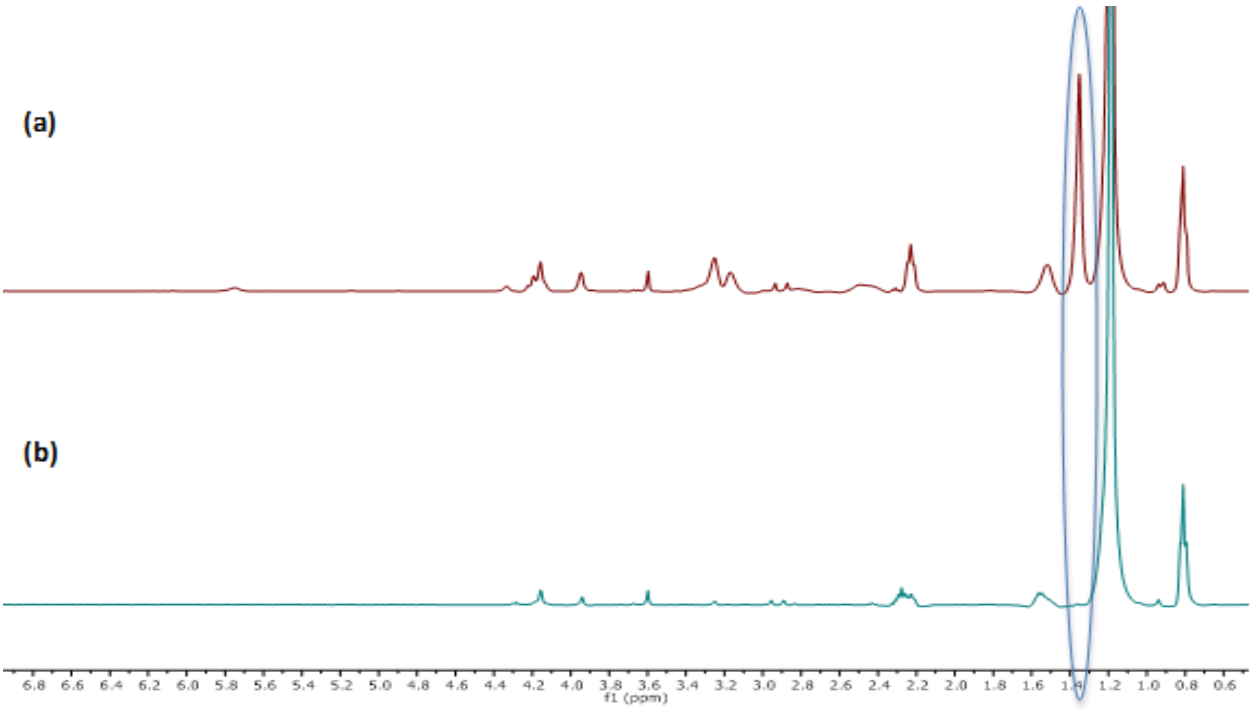

Figure S26. ^{1}H NMR comparison for (a) FA-PAMAM-BOC, (b) FA-PAMAM-NH_3^+ (500 MHz, $CDCl_3$)

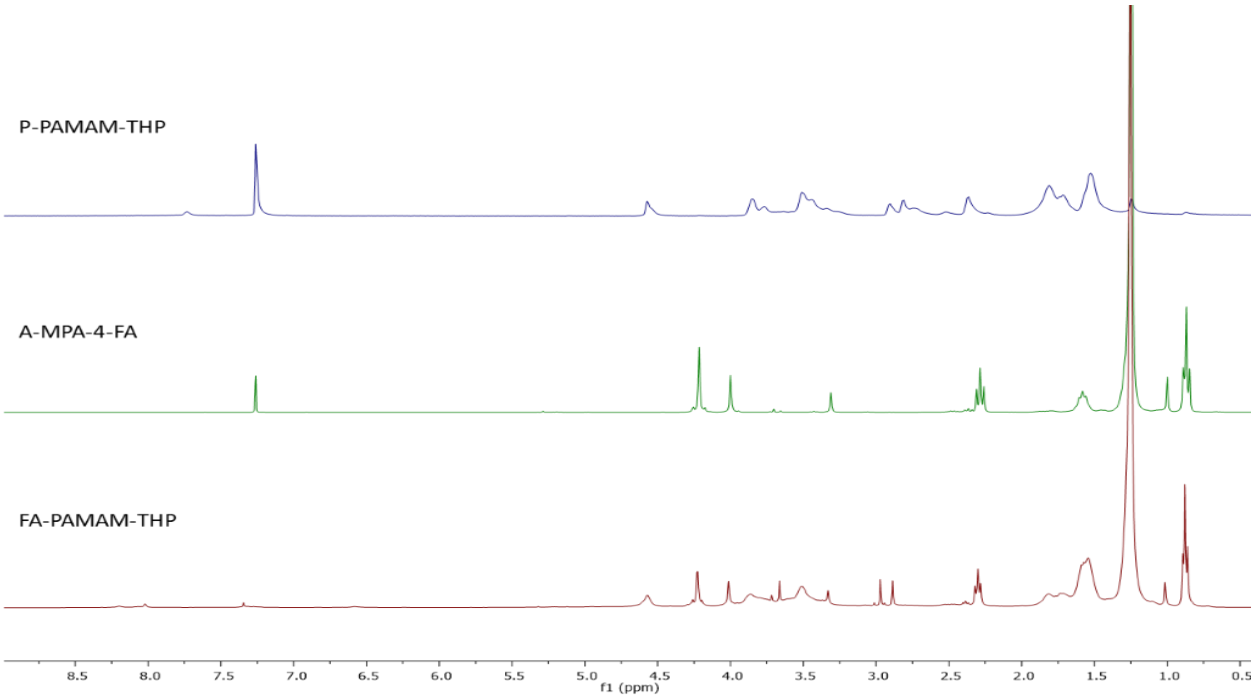

Figure S27. ^{1}H NMR comparison for FA-PAMAM-THP with P-PAMAM-THP and A-MPA-4-FA (500 MHz, $CDCl_3$)

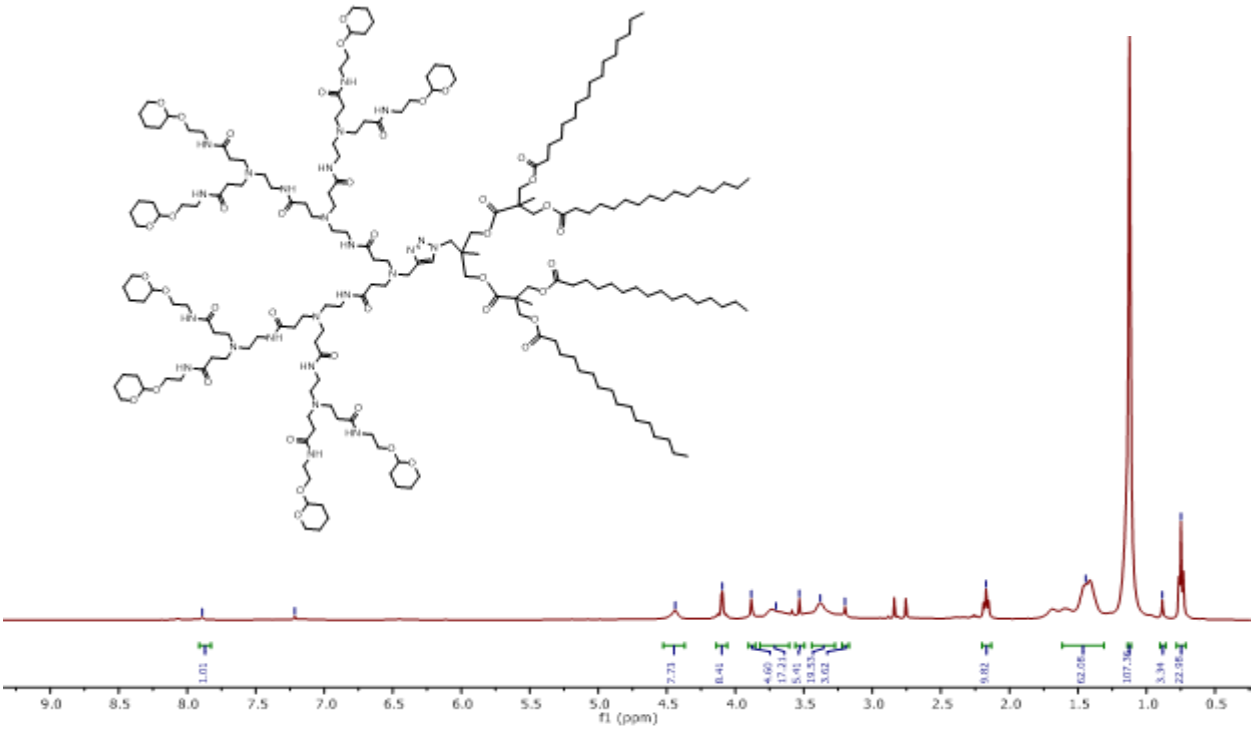

Figure S28. ^{1}H NMR for FA-PAMAM-THP (500 MHz, $CDCl_3$)

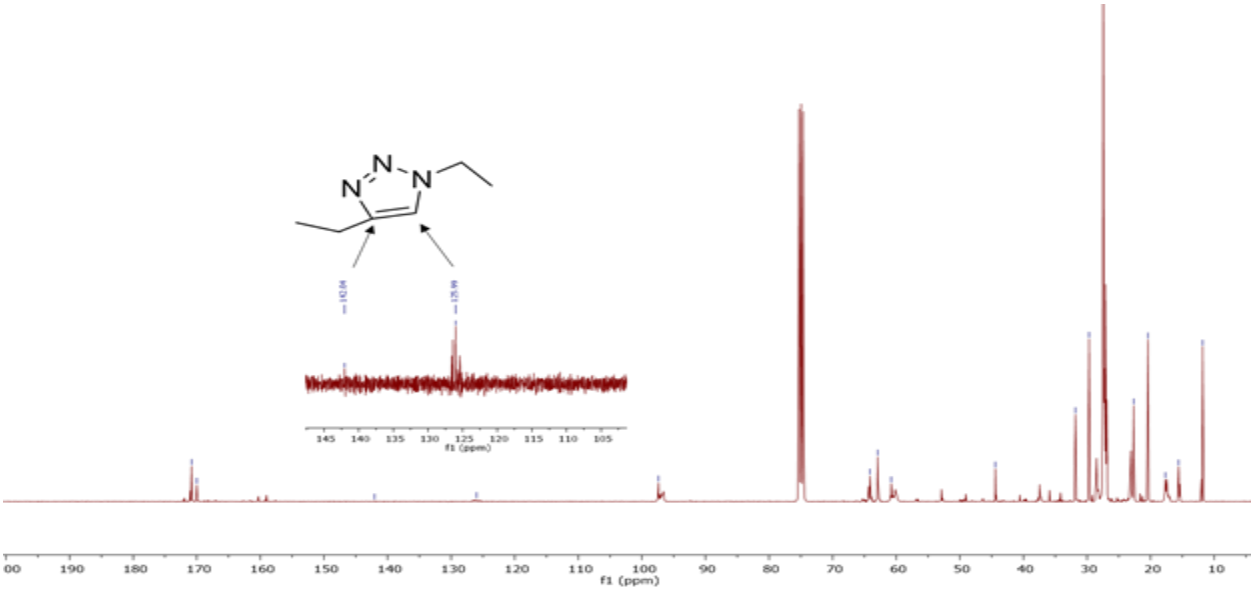

Figure S29. ^{13}C NMR for FA-PAMAM-THP (400 MHz, $CDCl_3$)

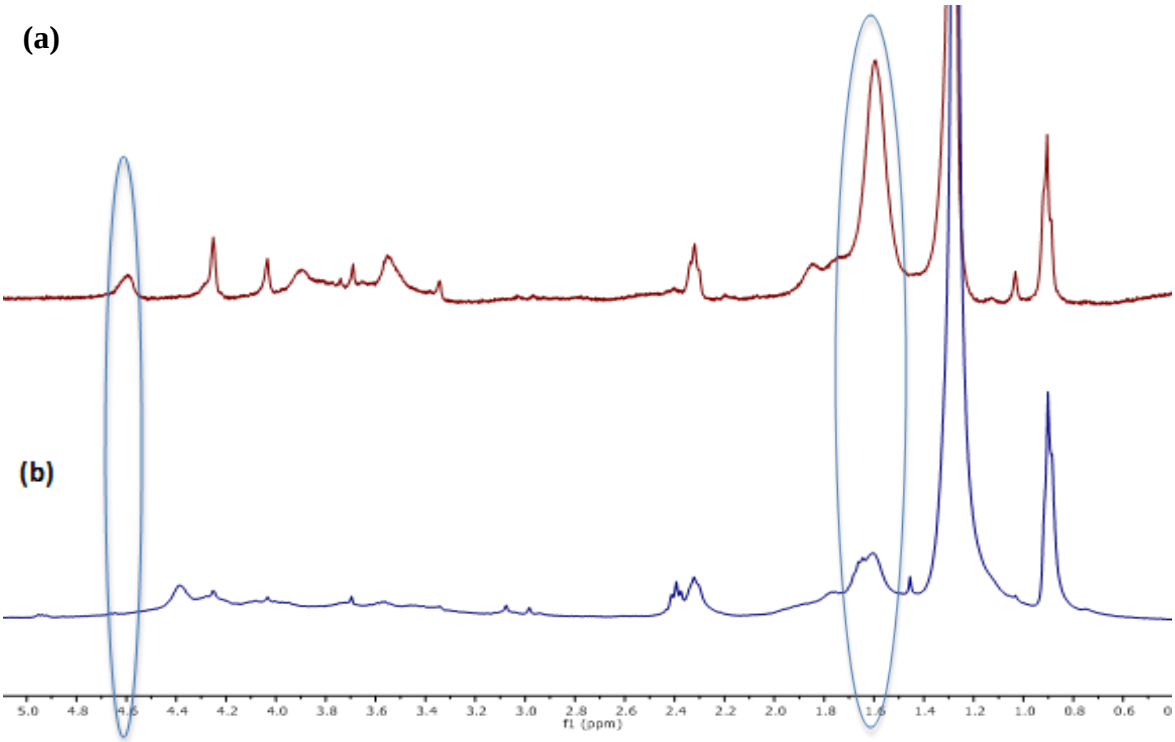

Figure S30. ^{1}H NMR comparison for (a) FA-PAMAM-THP, (b) FA-PAMAM-OH (500 MHz, $CDCl_3$

GPC CHROMATOGRAPHS

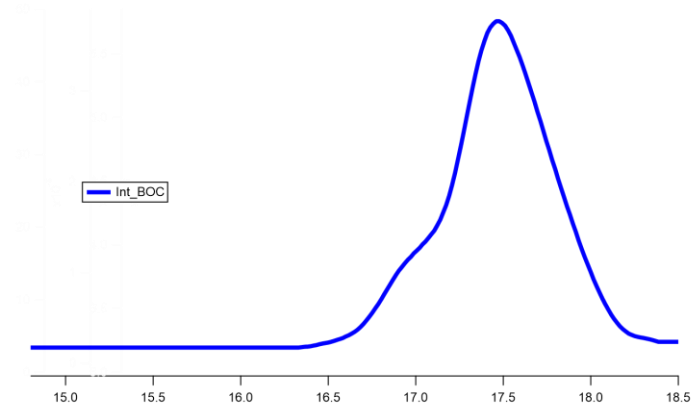

Figure S31. GPC chromatograms for 4-FA-PAMAM-BOC in THF

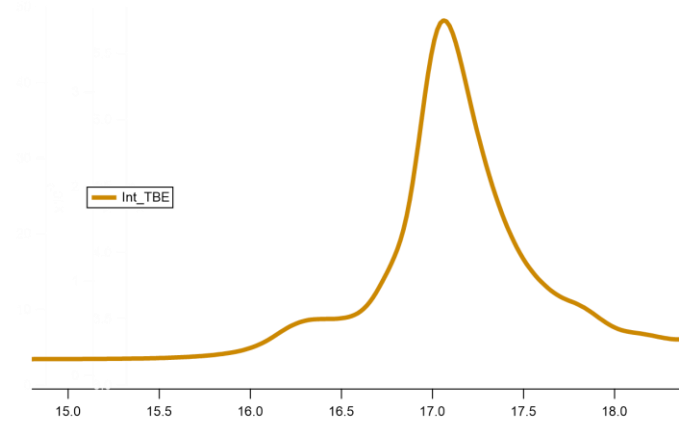

Figure S32. GPC chromatograms for 4-FA-PAMAM-TBE in THF

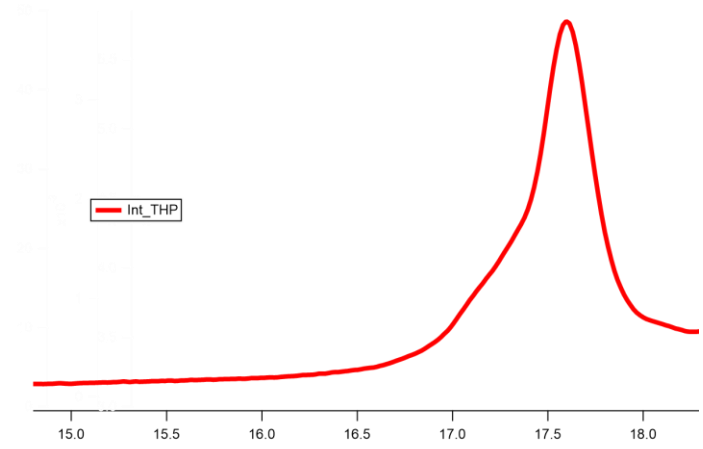

Figure S30. GPC chromatograms for 4-FA-PAMAM-THP in THF

DLS SPECTRA

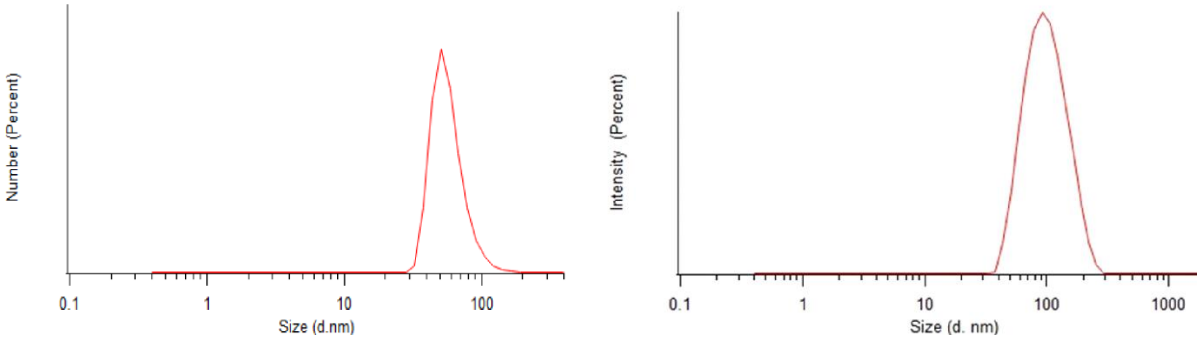

Figure S31. DLS spectra for FA-PAMAM-G3-NH_3^+, left: Size distribution by number, right: Size distribution by intensity

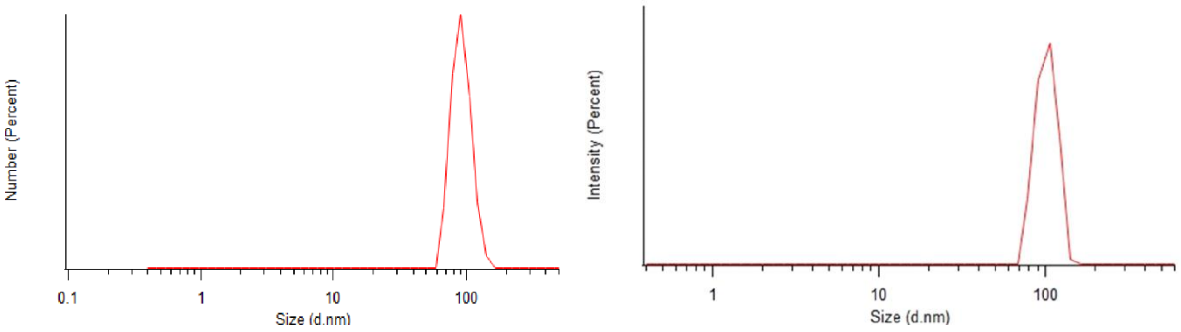

Figure S32. DLS spectra for FA-PAMAM-G3-COO^-, left: Size distribution by number, right: Size distribution by intensity

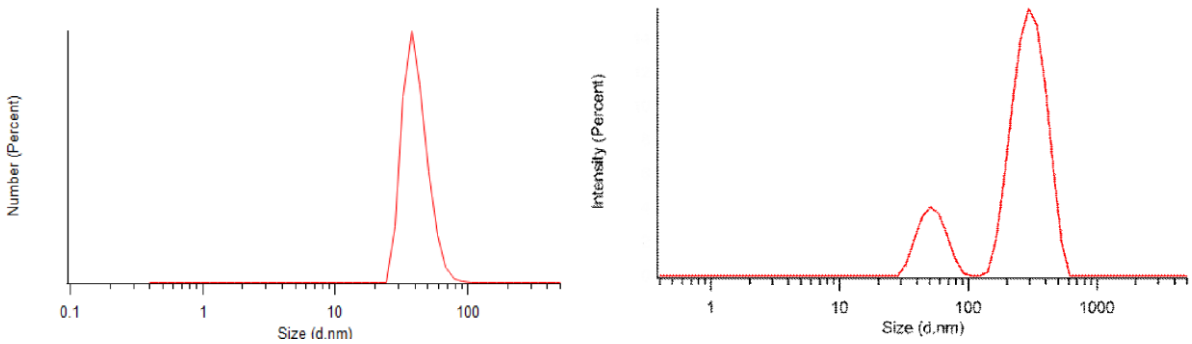

Figure S33. DLS spectra for FA-PAMAM-G3-OH, left: Size distribution by number, right: Size distribution by intensity

CAC DATA

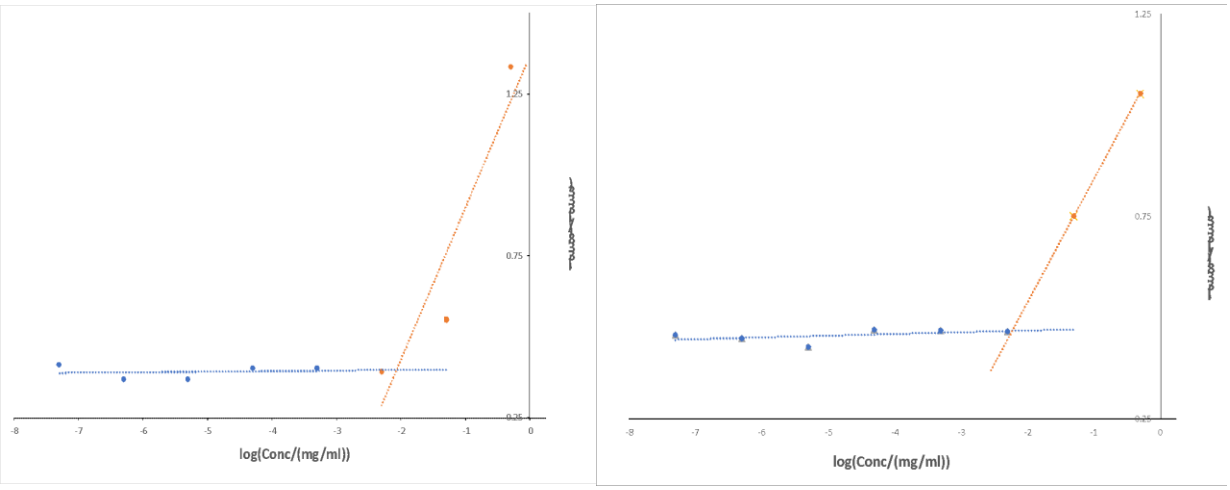

Figure S34. Excitation ratio vs. log concentration for FA-PAMAM-G3-NH_3^+ (left) and FA-PAMAM-G3- COO^- (right)

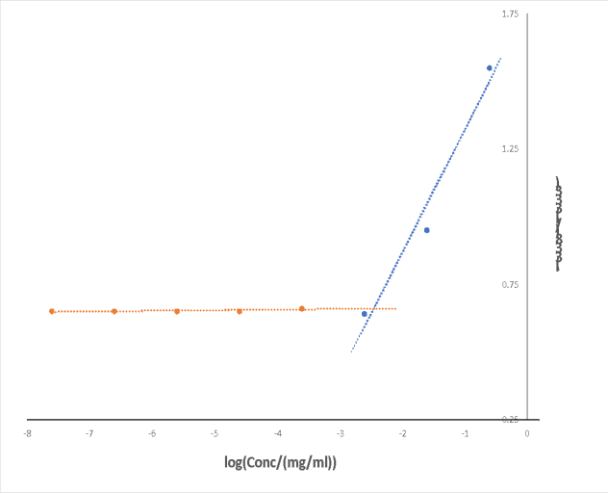

Figure S35. Excitation ratio vs. log concentration for FA-PAMAM-G3-OH

LIST OF REFERENCES

1. Kalhapure, Rahul S., et al. “Nanoengineered Drug Delivery Systems for Enhancing Antibiotic Therapy.” *Journal of Pharmaceutical Sciences*, vol. 104, no. 3, 2015, pp. 872–905., doi:10.1002/jps.24298.
2. Esfand, Roseita, and Donald A. Tomalia. “Poly(Amidoamine) (PAMAM) Dendrimers: from Biomimicry to Drug Delivery and Biomedical Applications.” *Drug Discovery Today*, vol. 6, no. 8, 2001, pp. 427–436., doi:10.1016/s1359-6446(01)01757-3.
3. Rigon, Roberta Balansin, et al. “Nanotechnology-Based Drug Delivery Systems for Melanoma Antitumoral Therapy: A Review.” *BioMed Research International*, vol. 2015, 2015, pp. 1–22., doi:10.1155/2015/841817.
4. Selin, Markus, et al. “Dendrimers and Their Supramolecular Nanostructures for Biomedical Applications.” *Journal of Drug Delivery Science and Technology*, vol. 34, 2016, pp. 10–20., doi:10.1016/j.jddst.2016.02.008.
5. Oliveira, Joaquim Miguel, et al. “Dendrimers and Derivatives as a Potential Therapeutic Tool in Regenerative Medicine Strategies—A Review.” *Progress in Polymer Science*, vol. 35, no. 9, 2010, pp. 1163–1194., doi:10.1016/j.progpolymsci.2010.04.006.
6. “PAMAM Dendrimers.” *Dendritech*, www.dendritech.com/pamam.html.

7. Tomalia, Donald A., et al. “Dendritic Macromolecules: Synthesis of Starburst Dendrimers.” *Macromolecules*, vol. 19, no. 9, 1986, pp. 2466–2468., doi:10.1021/ma00163a029.

8. Sikwal, Dhiraj R., et al. “An Emerging Class of Amphiphilic Dendrimers for Pharmaceutical and Biomedical Applications: Janus Amphiphilic Dendrimers.” *European Journal of Pharmaceutical Sciences*, vol. 97, 2017, pp. 113–134., doi:10.1016/j.ejps.2016.11.013.

9. Percec, V., et al. “Self-Assembly of Janus Dendrimers into Uniform Dendrimersomes and Other Complex Architectures.” *Science*, vol. 328, no. 5981, 2010, pp. 1009–1014., doi:10.1126/science.1185547.

10. Peterca, Mihai, et al. “Predicting the Size and Properties of Dendrimersomes from the Lamellar Structure of Their Amphiphilic Janus Dendrimers.” *Journal of the American Chemical Society*, vol. 133, no. 50, 2011, pp. 20507–20520., doi:10.1021/ja208762u.

11. Chandrasiri, Indika. “Synthesis and Characterization of Polylactide-PAMAM ‘Janus-Type’ Linear-Dendritic Hybrids.” *Journal of Polymer Science. Part A, Polymer Chemistry*, vol. 57, no. 13, 1 July 2019, pp. 1448–1459., doi: 10.1002/pola.29409.

12. Fox, Laura J., et al. “PAMAM Dendrimer - Cell Membrane Interactions.” *Advances in Colloid and Interface Science*, vol. 257, 2018, pp. 1–18., doi:10.1016/j.cis.2018.06.005.

13. Carvalho, Carla De, and Maria Caramujo. “The Various Roles of Fatty Acids.” *Molecules*, vol. 23, no. 10, 2018, p. 2583., doi:10.3390/molecules23102583.

14. Zhu, Chunlei, et al. “Reconstitution of Low-Density Lipoproteins with Fatty Acids for the Targeted Delivery of Drugs into Cancer Cells.” *Angewandte Chemie*, vol. 129, no. 35, 2017, pp. 10535–10538., doi:10.1002/ange.201704674.

15. Hernández-Ainsa, Silvia, et al. “Self-Assembly Modulation in Ionic PAMAM Derivatives.” *Soft Matter*, vol. 10, no. 2, 2014, pp. 281–289., doi:10.1039/c3sm52393d.

16. García-Gallego, Sandra, et al. “Fluoride-Promoted Esterification with Imidazolide-Activated Compounds: A Modular and Sustainable Approach to Dendrimers.” *Angewandte Chemie*, vol. 127, no. 8, 2015, pp. 2446–2449., doi:10.1002/ange.201411370.

17. Bugno, Jason, et al. “Tweaking Dendrimers and Dendritic Nanoparticles for Controlled Nano-Bio Interactions: Potential Nanocarriers for Improved Cancer Targeting.” *Journal of Drug Targeting*, vol. 23, no. 7-8, 2015, pp. 642–650., doi:10.3109/1061186x.2015.1052077.

18. Fröhlich, Eleonore. “The Role of Surface Charge in Cellular Uptake and Cytotoxicity of Medical Nanoparticles.” *International Journal of Nanomedicine*, 2012, p. 5577., doi:10.2147/ijn.s36111.

19. Kobayashi, Kenya, et al. “Surface Engineering of Nanoparticles for Therapeutic Applications.” *Polymer Journal*, vol. 46, no. 8, 2014, pp. 460–468., doi:10.1038/pj.2014.40.

20. Ozpolat, B., et al. “Nanomedicine Based Approaches for the Delivery of SiRNA in Cancer.” *Journal of Internal Medicine*, vol. 267, no. 1, 2010, pp. 44–53., doi:10.1111/j.1365-2796.2009.02191.x.

21. Araújo, Renan, et al. “New Advances in General Biomedical Applications of PAMAM Dendrimers.” *Molecules*, vol. 23, no. 11, 2018, p. 2849., doi:10.3390/molecules23112849.

22. Wang, Tao, et al. “Design, Synthesis, and Biological Evaluations of Asymmetric Bow-Tie PAMAM Dendrimer-Based Conjugates for Tumor-Targeted Drug Delivery.” *ACS Omega*, vol. 3, no. 4, 2018, pp. 3717–3736., doi:10.1021/acsomega.8b00409.

23. Kesharwani, Prashant, et al. “PAMAM Dendrimers as Promising Nanocarriers for RNAi Therapeutics.” *Materials Today*, vol. 18, no. 10, 2015, pp. 565–572., doi:10.1016/j.mattod.2015.06.003.

24. Stepto, Robert F. T. “Dispersity in Polymer Science (IUPAC Recommendations 2009).” *Pure and Applied Chemistry*, vol. 81, no. 2, 2009, pp. 351–353., doi:10.1351/pac-rec-08-05-02.

25. Shukla, S. K., et al. “Biodegradable Polymeric Nanostructures in Therapeutic Applications: Opportunities and Challenges.” *RSC Advances*, vol. 6, no. 97, 2016, pp. 94325–94351., doi:10.1039/c6ra15764e.

26. Lu, Boting, et al. “Chitosan-Modified PLGA Nanoparticles for Control-Released Drug Delivery.” *Polymers*, vol. 11, no. 2, 2019, p. 304., doi:10.3390/polym11020304.

27. Owen, Shawn C., et al. “Polymeric Micelle Stability.” *Nano Today*, vol. 7, no. 1, 2012, pp. 53–65., doi:10.1016/j.nantod.2012.01.002.

28. Lancelot, Alexandre, et al. “Nanostructures Based on Ammonium-Terminated Amphiphilic Janus Dendrimers as Camptothecin Carriers with Antiviral Activity.” *European Polymer Journal*, vol. 90, 2017, pp. 136–149., doi:10.1016/j.eurpolymj.2017.03.012.

29. Banik, Brittany L., et al. “Polymeric Nanoparticles: the Future of Nanomedicine.” *Wiley Interdisciplinary Reviews: Nanomedicine and Nanobiotechnology*, vol. 8, no. 2, 2015, pp. 271–299., doi:10.1002/wnan.1364.

30. He, Chunbai, et al. “Effects of Particle Size and Surface Charge on Cellular Uptake and Biodistribution of Polymeric Nanoparticles.” *Biomaterials*, vol. 31, no. 13, 2010, pp. 3657–3666., doi:10.1016/j.biomaterials.2010.01.065.

31. Mozar, Fitya Syarifa, and Ezharul Hoque Chowdhury. “Impact of PEGylated Nanoparticles on Tumor Targeted Drug Delivery.” *Current Pharmaceutical Design*, vol. 24, no. 28, 2018, pp. 3283–3296., doi:10.2174/1381612824666180730161721.

32. Chung, Tsai-Hua, et al. “The Effect of Surface Charge on the Uptake and Biological Function of Mesoporous Silica Nanoparticles in 3T3-L1 Cells and Human Mesenchymal Stem Cells.” *Biomaterials*, vol. 28, no. 19, 2007, pp. 2959–2966., doi:10.1016/j.biomaterials.2007.03.006.